Multi-robot Coverage and Exploration on Riemannian Manifolds with Boundary

Subhrajit Bhattacharya Robert Ghrist Vijay Kumar

Abstract

Multi-robot coverage and exploration are fundamental problems in robotics. A widely-used, efficient and distributable algorithm for achieving coverage of a convex environment with Euclidean metric is that proposed by Cortes, *et al.*, which is based on the discrete-time Lloyd's algorithm. This algorithm is not directly applicable to general Riemannian manifolds with boundary that non-convex and are intrinsically non-Euclidean. In this paper we generalize the control law based on minimization of the *coverage functional* to such non-Euclidean spaces punctured by obstacles. We also propose a practical discrete implementation based on standard graph search-based algorithms. We demonstrate the applicability of the proposed algorithm by solving efficient coverage problems on a sphere and a torus with obstacles, and exploration problems in non-convex indoor environments. [†]

1 Introduction

The geometry underlying configuration spaces of multiple robots is a critical feature implicit in several important challenges in planning and coordination. Metric considerations are fundamental to problems of coverage [Lloyd 82, Cortez 05, Cortez 04, Bullo 09], exploration [Thrun 05, Stachniss 05, Stachniss 06], and more. A well-known approach to solving coverage problems with n robots involve partitioning the appropriate configuration space into n-*tessellation* (a partition of the configuration space into simply-connected domains) [Lloyd 82, Cortez 05]. In particular, this method requires a Voronoi tessellation on the configuration space geometry. While such a tessellation is easy to achieve in a convex environment with Euclidean metric, it becomes increasingly difficult in environments with obstacles and non-Euclidean metrics. The presence of obstacles makes it a geodesically non-convex manifold with boundaries. Non-Euclidean metrics can arise in the geometry of a configuration space as inherited from the structure of the underlying domain (*e.g.*, from irregular terrain), or via direct manipulation of the configuration space geometry for problem goals (*e.g.*, in multi-robot cooperative exploration problems [Bhattacharya 10]).

The problem of attaining balanced coverage of an environment is fundamental to many practical multi-robot problems. One common coverage control approach — efficient and distributable — is through the definition of feedback control laws defined with respect to the centroids of Voronoi cells resulting from the Voronoi tessellation of the domain. Lloyd's algorithm [Lloyd 82] is a discrete-time algorithm that minimizes a *coverage functional*. A continuous-time version of the algorithm is described in [Cortes 04], where the authors propose gradient descent-based individual robot control laws that guarantee optimal coverage of a convex environment given a density function which

[†]Parts of this work have been presented at the 10^{th} International Workshop on the Algorithmic Foundations of Robotics (WAFR), 2012.

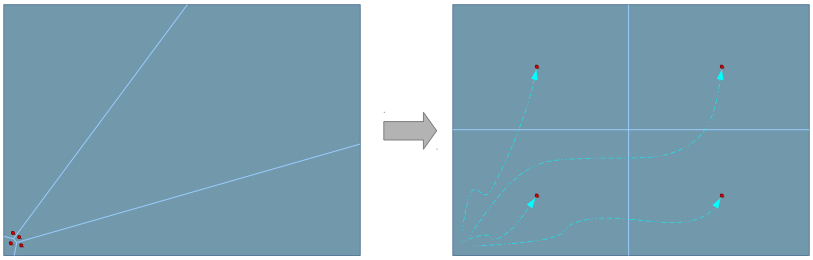

(a) The algorithm due to Cortes, *et al.* for attaining uniform coverage in a convex environment with Euclidean metric.

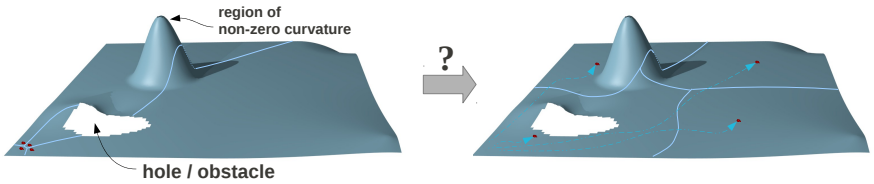

(b) We would like to solve the problem for a geodesically non-convex Riemannian manifold with boundary.

Figure 1: An overview of the main contribution of the paper.

represents the desired coverage distribution. To remove the limiting assumption of a convex environment, the authors of [Pimenta 08] propose the use of *geodesic Voronoi tessellation* determined by the geodesic distance rather than the Euclidean distance. However such a method both involves computationally-difficult geometric computations and is still limited to Euclidean environments with polygonal obstacles. Recent work [Bhattacharya 10] has used a graph search-based approach to develop tools for solving the coverage problem in non-convex environments with a non-Euclidean metric. However, in order to explicitly compute an analog of a *generalized centroid* in non-convex tessella, an approximate method involving *centroid projection* was used. Such a method is, admittedly ad hoc, gives weak guarantees, and is difficult to implement when the configuration space is not topologically simple (equivalent to a punctured simply-connected domain). There exist search-based discrete-time algorithms that explicitly search every vertex in a tessellation to find the best position for the robot in every time-step (as in [Durham 12]). Although such a controller can solve the problem of multi-robot decentralized coverage on arbitrary metric graphs, the high computational complexity of this approach makes it impractical for fine discretization or large graphs.

Contributions and Organization:

In this paper we generalize the method for computing the control law that is described in [Pimenta 08, Lloyd 82] and adapt it to non-Euclidean metric spaces with obstacles that are not necessarily polygonal (Figure 1). The principal theoretical tool is Proposition P1, with Corollary C1 giving an explicit formula ready for computation. They relate geodesics, distance derivatives, and the metric tensor. However, the computability relies on the existence of minimal paths and differentiability of the distance function. These are formally discussed in details in Section 2.2 and Lemma L2. This inspires the design of the control law in Equation (7). This control law does not suffer from the issues of 'local minima' due to presence of obstacles because of the fact that we use the *length metric* as our distance function. This is formally proved in Section 3 using Proposition P1 and Lemma L1. We realize the control law using a graph search-based method to achieve an efficient

discrete implementation. We illustrate our methodology by showing how to solve Coverage problems on non-Euclidean Riemannian manifolds with boundary, multi-robot cooperative exploration, and cooperative human-robot exploration.

In Section 2 of the paper we primarily discuss some mathematical tools related to Riemannian manifolds with boundary. The main contribution of the paper appears in Section 3 where we develop and prove stability of the proposed control law for coverage on Riemannian manifolds with boundary. We present the graph search-based discrete implementation and simulation results in Section 4. For better readability, we have placed the proofs of the lemmas, the corollary and the proposition in the paper in the appendix at the end of the paper.

2 Background – Manifolds with Boundary

In this section we discuss and build some of the theoretical tools that will be essential in designing and proving the stability of the control law (which we will do in Section 3) for coverage in general Riemannian manifolds with boundary.

2.1 Motivation: Stability and Convergence of Control Laws

If the configuration space of a robot (or a system of robots) can be described by a Banach space (*i.e.* a vector space with a norm, $\|\cdot\|$), one can easily specify convergence and stability of a proposed control law. In particular, Lyapunov stability, asymptotic stability and exponential stability [Sastry 99] are some of the conditions that are often desired. These stability analyses often boil down to finding an energy-like function (often called the *Lyapunov function*), and showing that the proposed control law can be expressed as the gradient of the energy-like function. Conditions on the function and its gradients on the entire space translate into stability conditions.

However, very often the configuration space under consideration is a general Riemannian manifold. If it is a complete manifold (*i.e.* every geodesic curve on it can be extended indefinitely in both directions), one approach is to consider the tangent space at a point [Petersen 06], which is a Hilbert space (and hence a Banach space), and study the local stability of the control laws in the tangent space via the exponential map. Since the exponential map is often not bijective, especially for compact manifolds, the study of convergence in terms of Lyapunov function makes sense only locally at each point.

However the scenario is most difficult when the manifold is not complete. These are typically manifolds obtained by removing closed sets from other complete manifolds. In such cases the exponential map is not even defined completely on the entire tangent space at a point. Geodesic emanating from a point can hit a hole/puncture on the manifold. We often include the boundary near the holes/punctures to make it a *manifold with boundaries*. That makes it complete as a metric space, but it no longer remains a manifold since the points at the boundary do not locally resemble Euclidean space. Thus we lose the notion of a tangent bundle on this space with the tangent space being fibers that are identical at every point.

Unfortunately it is the last kind of spaces that one encounters most often in problems of robot navigation. The holes or punctures arise due to presence of obstacles. Supposing one can embed the manifold with boundaries in an Banach space, stability of control laws on the embedding space does not correspond to stability on the manifold with punctures.

The simplest example is that of a point robot navigating on $\mathbb{R}^2$, and the objective being reaching a goal point, $\mathbf{p}_g \in \mathbb{R}^2$. One can simply construct a smooth energy function, $\mathcal{E} : \mathbb{R}^2 \to \mathbb{R}$, with an unique global minima at $\mathbf{p}_g$, and non-zero gradient everywhere else (*e.g.* $\mathcal{E}(\mathbf{r}) = \|(\mathbf{r} - \mathbf{p}_g)\|^2$). The

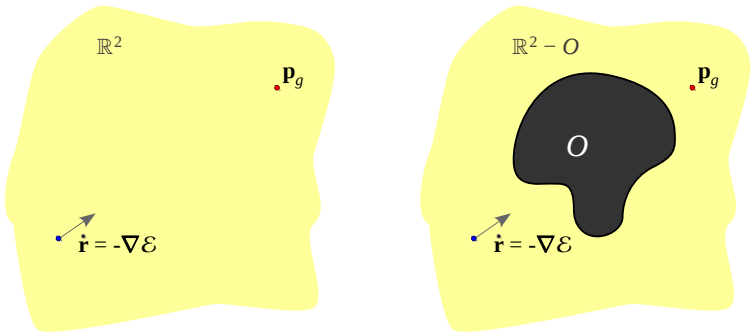

(a) Point robot at $\mathbf{r}$ navigating towards $\mathbf{p}_g$ in the Banach space, $\mathbb{R}^2$, by descending gradient of $\mathcal{E}$, will reach its goal.

(b) $\mathbb{R}^2 - O$ is not a Banach space. On this space the integral curve of $\dot{\mathbf{r}} = -\nabla\mathcal{E}$ does not exist.

Figure 2: In presence of obstacles, a robot can get stuck at '*local minima*' at the boundary of the obstacles. This is because of the fact that the control vector at a point on the boundary may not exist inside the *tangent cone* at the point, and hence tend to 'push' the robot into obstacles.

robot following the negative of the gradient of this function would reach the goal (*i.e.* the integral curve of $\dot{\mathbf{r}} = -2(\mathbf{r} - \mathbf{p}_g)$, exists in $\mathbb{R}^2$, and converges to $\mathbf{p}_g$ as $t \to \infty$, the convergence being exponential in this particular example – Figure 2(a)). However, if we remove an open subset O from $\mathbb{R}^2$ and make that the configuration space of the robot, the same control law will end up making the robot hit the boundary of O and 'get stuck' there, since the control action will tend to make the robot move into O (Figure 2(b)). These are typically referred to as '*local minima*' in robotics literature. However, the more fundamental reason that these kinds of minima occur is that the control vector may not always belong to the *tangent cone* (an analog of the tangent space: see Section 2.3) at the point on the boundary.

To solve this problem, one may attempt to generate a smooth energy function in $\mathbb{R}^2$ such that, starting at any point in $\mathbb{R}^2 - O$, the integral curves of the gradient of the function will remain completely inside $\mathbb{R}^2 - O$. This was the approach adopted in [Rimon 92], which involved the construction of specially crafted *navigation functions*. However, the construction of such energy functions is, in general, difficult, computationally expensive and works only for special classes of obstacles, O. The other, more direct approach in $\mathbb{R}^2$ involves the construction of visibility graphs [Lozano-Pérez 79]. In this approach the robot essentially follows the shortest path that lies entirely in the free configuration space. This, in effect, generates a vector field with the property of integral curves lying entirely in $\mathbb{R}^2 - O$ as desired.

While the direct construction of this vector field is simple in case of the problem of goal-directed navigation for a single robot, very often one is faced with an objective that is more naturally described in terms of minimization of an energy function. The problem of robot coverage [Lloyd 82, Cortez 05, Cortez 04, Bullo 09] is one such problem we will consider extensively later in this paper. In such problems it is natural to compute the control commands from the gradient of the energy-like functions. So the more general question that arises is:

> What class of energy-like functions defined on a manifold, Ω, possibly with boundary, will guarantee that the integral curves of their gradients, starting from a point in Ω, will completely lie inside Ω? What can we say about the convergence/stability of the

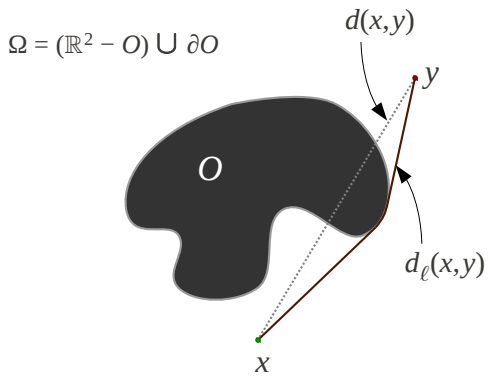

Figure 3: In this figure O represents a compact obstacle with smooth boundary in $\mathbb{R}^2$. $\Omega = (\mathbb{R}^2 - O) \cup \partial O$ is a manifold with smooth boundary that is complete as a metric space. The metric induced by $\mathbb{R}^2$ is not a path metric since a path of length $d(x, y)$ does not exist in Ω. But d_ℓ is a path metric.

system?

While in this paper we will mostly focus on the problem of multi-robot coverage, we hope that the analysis that we will present in the following sections will help in establishing a much broader control paradigm on manifolds with boundary.

2.2 Length Metric

We consider a smooth manifold, Ω, possibly with boundary. Such spaces are well-studied in mathematics [Wolter 85, Alexander 81]. In robotics they are of great interest since they represent configuration spaces of many robots and linkages with no "immaterial edge" assumptions. For most of the analysis in this paper we will assume that Ω is embedded in some Euclidean space equipped with its standard Euclidean metric $(\mathbb{R}^D, d)$. The topology of Ω is assumed to be the *subspace topology* [Munkres 99] derived from $\mathbb{R}^D$ (so that the boundary of Ω is part of the same topological space). The metric induced by the ambient Euclidean space is, in general, not a *path metric* unless Ω is convex (see p.10 of [Gromov 99]). That means, if $i : \Omega \hookrightarrow \mathbb{R}^D$ is the embedding, for any points $p, q \in \Omega$, there may not exist a path $[0, 1] \to \Omega$ of length $d(i(p), i(q))$.

However, if Ω is path connected, one can define a different metric structure on Ω that makes it a path metric space, (Ω, d_ℓ). The new metric, d_ℓ, called the *length metric*, can be defined such that $d_\ell(p, q)$ is the infimum of the length of *rectifiable* curves or paths (computed using the *length structure* [Gromov 99] induced by the embedding) joining p and q, but lying entirely in Ω. It is not difficult to see that (Ω, d_ℓ) is a complete metric space (though not geodesically complete). Thus, due to the Hopf-Rinow theorem [Gromov 99] there exists a minimizing path (not necessarily unique) joining every pair of points. Although this last observation may appear somewhat trivial, it is easy to construct cases of non-compact manifolds where such minimizing geodesics may not exist (*e.g.*, in Figure 3, consider $\mathbb{R}^D - O$, without the boundary of O – a path of length equal to the infimum does not exist in that space for the shown points x, y). Thus we cannot simply remove the boundaries from the space of interest.

2.3 Generalization of Tangent Space

By retaining the boundary, Ω no more remains a manifold in the strict sense. Neighborhoods of points on the boundary of Ω (*i.e.*, points on $\partial\Omega$) resemble an Euclidean half space. However, $\Omega - \partial\Omega$ is indeed a manifold, although not complete. Thus, given $p \in (\Omega - \partial\Omega)$, one can define the tangent space $T_p(\Omega - \partial\Omega)$ in its usual sense. However, we do not have the usual notion of a tangent space at points on $\partial\Omega$.

Let us now consider a point, $p \in \Omega$. The tangent space of the Euclidean space in which Ω is embedded is thus $T_{i(p)}\mathbb{R}^D$. Now we consider the subset of this tangent space that consists of the vectors (and their non-negative scalings) that are tangents to curves emanating from p and lying entirely in Ω. That is, we define the cone,

$$T_p\Omega = \bigcup_{v \in \Lambda_p\Omega} \{\alpha v \mid \alpha \geq 0\}$$

where,

$$\Lambda_p\Omega = \left\{ \left(\frac{d\gamma^i}{dt}\Big|_{t=0} \right) \frac{\partial}{\partial x^i} \;\middle|\; \begin{array}{l} \gamma : [0, a] \to \mathbb{R}^D, a > 0 \text{ are } C^1 \text{ paths parametrized by their lengths,} \\ \text{with } \gamma(0) = p,\ Img(\gamma) \subseteq \Omega \end{array} \right\}$$

Here trajectory, γ, has been represented using a coordinate system of choice on $\mathbb{R}^D$. We call $T_p\Omega$ the *tangent cone* at p in Ω.

Lemma L1. *If Ω is a smooth manifold embedded in $\mathbb{R}^D$, $T_p\Omega$ is a half space in $T_{i(p)}\mathbb{R}^D$ for $p \in \partial\Omega$, and a full space for $p \in (\Omega - \partial\Omega)$ (see Figure 4).*

Remark R1. The above lemma can be generalized to assert that $T_p\Omega$ will be a convex cone for points on a wider class of manifolds with boundaries with corners (*i.e.* boundaries that are not necessarily smooth). As long as the space is locally convex (*i.e.* for every point $p \in \Omega$, there exists a open neighborhood, U, in Ω, such that the metric induced by d makes U a path metric space), $T_p\Omega$ will be a convex cone (Figure 4(c)).

Remark R2. We will allow $\partial\Omega$ to be not smooth (C^1) at finite number of distinct points, where they may not be locally convex either. In our coverage problem such a point can at the worst be an unstable 'local minima', in which case we will rely on presence of small noise that would 'push' the robot out that isolated point (see Section 3). Alternatively we can assume smoothness of the boundary to be a generic condition, wherein a boundary with finite and distinct set of non-smooth points can be *smoothened* locally (using a *mollifier*) to obtain a C^1 boundary. In which case the result of Lemma L1 will hold for every point.

Remark R3. We define the *cotangent cone* at p as the dual of the cone $T_p\Omega$, and represent it as $T_p^*\Omega$. If $T_p\Omega$ is convex, so is $T_p^*\Omega$, and vise-versa. Consider a real-valued smooth function, $f : \Omega \to \mathbb{R}$. A differential of f is defined as an element of $T_p^*\Omega$ in usual way at points that lie in $(\Omega - \partial\Omega)$. To define a differential at a point p that lies on $\partial\Omega$, we take a Cauchy sequence of points in $\Omega - \partial\Omega$ that converges to p (recall that Ω is a complete metric space). The limit of the differentials of f in the cotangent cones of these points gives us the required differential at p. This limit, however, may or may not exists in $T_p^*\Omega$, and that will depend on the nature of f. The gradient of f is the corresponding dual of the differential in $T_p\Omega$.

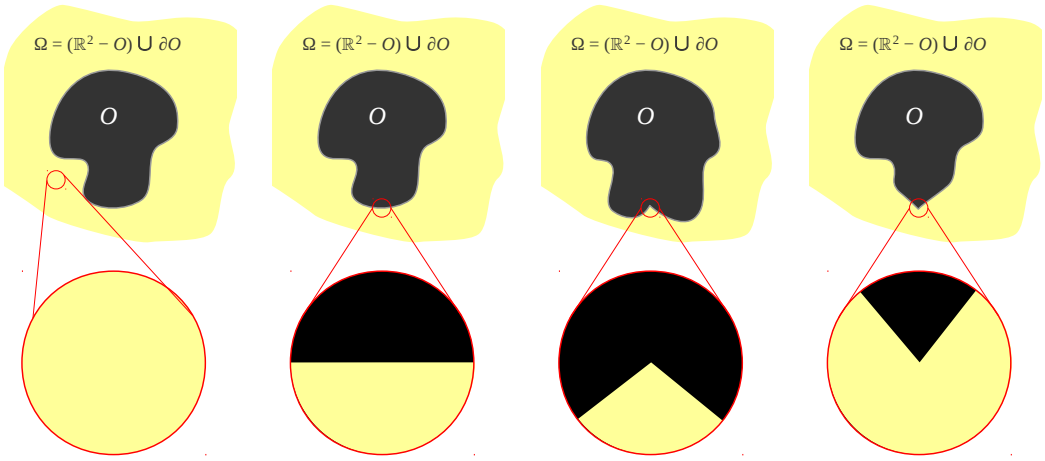

(a) In the interior of Ω, neighborhoods are Euclidean space, which is convex.

(b) On smooth boundary of Ω, neighborhoods are Euclidean half space, which is convex.

(c) Although this is a point on the boundary where it is not C^1, $T_p\Omega$ is still convex.

(d) $T_p\Omega$ is not convex at this point.

Figure 4: Points on Ω and the shape of $T_p\Omega$ (the pale yellow region inside the circle). (a), (b) show Ω with smooth boundary. (c), (d) show Ω with non-smooth boundary.

2.4 Cut Locus

Definition D1 (Cut locus on manifolds with boundary – See Definition 3.4.II of [Wolter 85])**.** Let $p \in \Omega$. A point, $q \in (\Omega - \partial\Omega)$, is called a *pica* relative to p if p and q can be joined with two or more distinct minimal paths (*i.e.* paths of length $d_\ell(p, q)$) with distinct tangents at q. The closure of the set of all picas relative to p is called the *cut locus* of p and is denoted by $\mathcal{C}_p$ (Figure 5(a)).

Note that by using the term 'distinct minimal paths' we mean to impose the condition that the image of any two distinct paths are not the same. This excludes the multiplicity of paths due to mere re-parameterization. The definition of cut locus in terms of 'pica' (equivalently, *non-extenders*) is necessary for retaining certain properties of the standard cut locus on manifolds without boundaries.

Lemma L2 (Wolter [Wolter 85])**.** *If Ω is a smooth manifold (with boundaries), which is complete as a metric space, and can be defined as a subset of a smooth, complete manifold of same dimension, then for every $p \in \Omega$,*

i. $\mathcal{C}_p$ is a closed set of measure zero in Ω,

ii. the function $g_p := d_\ell(p, \cdot)$ is of class C^1 in $\Omega - (\partial\Omega \cup p \cup \mathcal{C}_p)$, and

iii. the gradient of g_p is bounded in $\Omega - (\partial\Omega \cup p \cup \mathcal{C}_p)$.

Lemma L3. *For almost every point $p \in \Omega$:* $q \notin \mathcal{C}_p \implies p \notin \mathcal{C}_q$

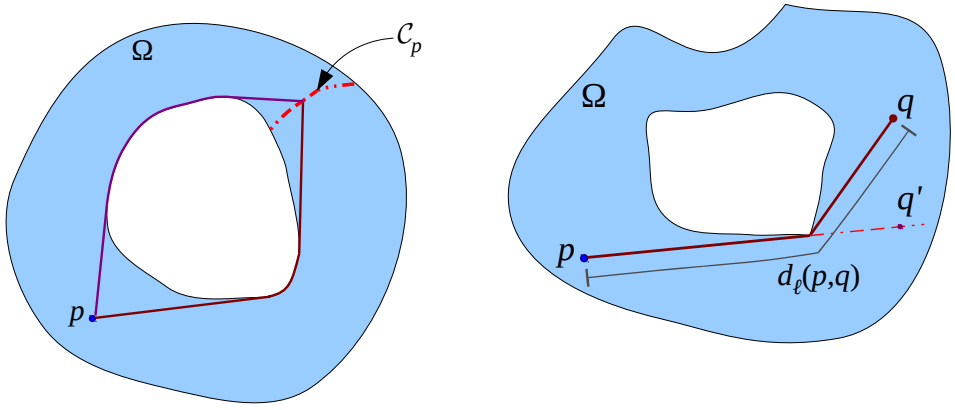

(a) Points on $\mathcal{C}_p$ can be joined with p using 2 minimal geodesics.

(b) On points on the dotted line in this figure (*e.g.* the point q'), g_p is C^1, but not C^2.

Figure 5: The cut locus of p and the smoothness of the function g_p.

2.5 Gradient of Distance Function

Proposition P1. *Let $p \in \Omega$. The negative of the gradient of $g_p := d_\ell(p, \cdot)$ exists in $T_q\Omega$ (equivalently, the negative of the differential of g_p exists in $T_q^*\Omega$) at all points $q \in \Omega - (p \cup \mathcal{C}_p)$ that are equipped with a Riemannian metric in their neighborhoods. The negative of the gradient is equal to a normalized vector at q along the tangent to the minimal path connecting q to p (equivalently, the differential is the dual of the unit tangent vector along the minimal path).*

Remark on existence: If q is a point in $\Omega - (\partial\Omega \cup p \cup \mathcal{C}_p)$, the gradient (and its negative) obviously exist in $T_q\Omega$ (part 'ii.' of Lemma L2). We need to check the existence for points on the boundary $\partial\Omega$. Recall that for points, $q \in \partial\Omega$, we defined the gradient of a function as the limit of the gradients over a Cauchy sequence of points, $\{q_n\}$, in $\Omega - (p \cup \partial\Omega \cup \mathcal{C}_p)$ converging to q. We can prove the later half of the statement for each of these q_n (*i.e.* that the negative of the gradient is equal to a normalized vector at q_n along the tangent to the minimal path connecting q_n to p). Then, the existence of the negative of the gradient at q is implied by the existence of the minimal path. Since the tangent to the minimal path connecting q to p exists in $T_q\Omega$ (by definition of the tangent cone), the negative of the gradient will also exist (see Figure 6).

Thus, the proof of the above proposition relies on being able to compute the gradient of g_p at $q \in \Omega - (p \cup \partial\Omega \cup \mathcal{C}_p)$ in terms of the tangent to the minimal path. Using the lemma and corollary that follows next, we will establish an explicit relationship between the gradient of g_p and tangents to minimal paths using a coordinate representation of the metric tensor, and using these will be able to prove the Proposition P1. We will assume summation over repeated indices following the Einstein summation convention, and coordinatize tangent spaces and the cotangent spaces by $\{\frac{\partial}{\partial x^i}\}_{i=1,2,\cdots,N}$ and $\{\mathrm{d}x^i\}_{i=1,2,\cdots,N}$ respectively [Jost 97, Petersen 06].

Notations: We will use regular italic letters to denote points and vectors (*e.g* $p \in \Omega$ and $u \in$

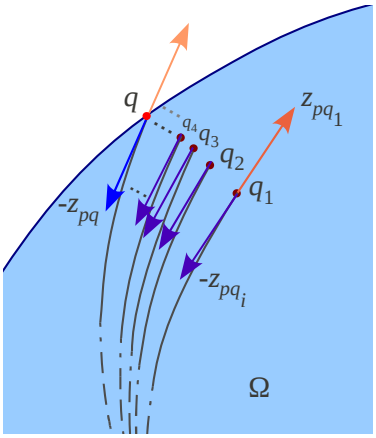

Figure 6: Illustration for Proposition P1. The gradient of g_p at $q \in \partial\Omega$ is the limit of $-z_{pq_i}$ as $i \to \infty$, where $q_1, q_2, \cdots$ is a Cauchy sequence converging to q.

$T_p\Omega$), and boldface to denote the coordinate representation of points (*e.g.*, $\mathbf{p} \in \mathbb{R}^N$) and coefficient vectors (*e.g.* $\mathbf{u} \in \mathbb{R}^N$) in a particular coordinate chart. Later in Section 4, we will use regular font to represent vertices in a discrete graph. We will typically use 'η' to denote the Riamannian metric tensor. Also, given a metric, d_*, on a manifold, M, and a coordinate chart $C = (U, \phi)$ on an open subset $U \subseteq M$, we define,

i. $d_*^C : \mathbb{R}^N \times \mathbb{R}^N \to \mathbb{R}$, the metric restricted to U and described in terms of the coordinate chart C, as $d_*^C(\mathbf{a}, \mathbf{b}) = d_*(\phi^{-1}(\mathbf{a}), \phi^{-1}(\mathbf{b})), \ \ \forall\, \mathbf{a}, \mathbf{b} \in Img(\phi)$, and,

ii. $d_*^{\tilde{C}} : M \times \mathbb{R}^N \to \mathbb{R}$, the metric with the second parameter restricted to U and described in terms of the coordinate chart C, as $d_*^{\tilde{C}}(a, \mathbf{b}) = d_*(a, \phi^{-1}(\mathbf{b})), \ \ \forall\, \mathbf{b} \in Img(\phi)$.

Lemma L4. *Let U be a geodesically convex open set in a N-dimensional Riemannian manifold (possibly with boundary) Ω, equipped with a Riemannian metric tensor, η, at every point. We also assume that for all $p \in U$, $\mathcal{C}_p$ is empty inside U. Let d be the metric on U, induced by the Riemannian metric tensor, η (which agrees with the length metric, d_ℓ, since U is geodesically convex).*

Then for every coordinate chart, $C = (U, \phi)$, defined on U (with coordinate variables $u^1, u^2, \cdots, u^D$), and every $w, q \in U$, with $\mathbf{w} = \phi(w), \mathbf{q} = \phi(q)$, the following is true (Figure 7(a)),

$$\left[\frac{\partial}{\partial \mathbf{u}} d^C(\mathbf{w}, \mathbf{u})\bigg|_{\mathbf{u}=\mathbf{q}}\right]_i \equiv \frac{\partial}{\partial u^i} d^C(\mathbf{w}, \mathbf{u})\bigg|_{\mathbf{u}=\mathbf{q}} = \frac{\eta_{ij}(\mathbf{q})\ z^j_{w\mathbf{q}}}{\sqrt{\eta_{mn}(\mathbf{q})\ z^m_{w\mathbf{q}} z^n_{w\mathbf{q}}}}$$

where, $\mathbf{z}_{w\mathbf{q}} = [z^1_{w\mathbf{q}}, z^2_{w\mathbf{q}}, \cdots, z^D_{w\mathbf{q}}]^T$ is the coefficient vector (in coordinate chart C) of the tangent vector at q to the shortest geodesic connecting w to q, and by $\left[\frac{\partial f}{\partial \mathbf{u}}\right]_i$ we mean the i^{th} component of $\left[\frac{\partial f}{\partial u^1}, \frac{\partial f}{\partial u^2}, \cdots, \frac{\partial f}{\partial u^D}\right]$.

If we define $g_{\mathbf{w}}(\mathbf{u}) := d^C(\mathbf{w}, \mathbf{u}), \ \forall \mathbf{u} \in Img(\phi)$ (*i.e.*, $g_{\mathbf{w}}(\mathbf{q})$ is the length of the shortest geodesic connecting w to q), the statement of the proposition essentially implies that the normals to the constant $g_{\mathbf{w}}$ surfaces are parallel to the dual of the tangents (cotangents) to the geodesics. This

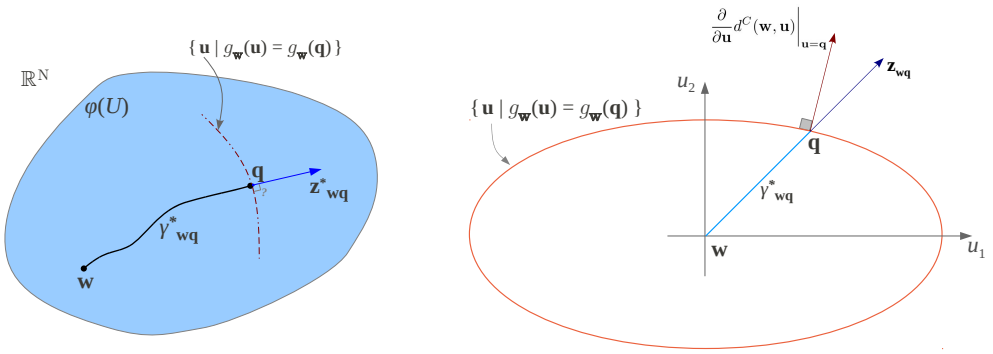

(a) Illustration for Lemma L4 showing the relationship between the tangent to the geodesic $\gamma^*_{\mathbf{wq}}$ at $\mathbf{q}$, and the normal to the surface $\{\mathbf{u}|g(\mathbf{u}) = g(\mathbf{q})\}$ at $\mathbf{q}$.

(b) Illustration in a simple non-Euclidean, anisotropic metric. Note that the normal to the ellipse is not parallel to the tangent to the geodesic, $\mathbf{z_{wq}}$. It is however parallel to the cotangent, $\mathbf{z^*_{wq}}$, with coefficients $z^*_{i,\mathbf{wq}} = \eta_{ij}(\mathbf{q})\, z^j_{\mathbf{wq}}$.

Figure 7: Relationship between tangent to a geodesic and the derivative of the distance function.

is illustrated in Figure 7(a). The statement of the proposition essentially expresses the gradient of the distance function d (with respect to one of its arguments) in terms of the tangent to the geodesic connecting two points.

Examples:

1. We note that when the metric tensor is Euclidean in the given chart (*i.e.* $\eta_{ij} = \delta_{ij}$ everywhere as was the case in [Pimenta 08]), the result of the proposition simply reduces to $\frac{\partial}{\partial u^i} d(\mathbf{w}, \mathbf{u})\big|_{\mathbf{u}=\mathbf{q}} = z^i_{\mathbf{wq}}$. This is no surprise since we know that the vector $\frac{\partial}{\partial \mathbf{u}} d(\mathbf{w}, \mathbf{u})\big|_{\mathbf{u}=\mathbf{q}}$ is essentially an unit normal to the sphere with center $\mathbf{w}$ (which is the surface of constant $d(\mathbf{w}, \mathbf{u})$) at the point $\mathbf{u} = \mathbf{q}$, which is well-known to be parallel to the straight line connecting $\mathbf{w}$ to $\mathbf{q}$ (a radial line of the sphere).

2. If the metric is locally isotropic in the given chart (*i.e.* if the matrix representation of the metric is a multiple of the identity matrix at every point), and can be written as $\eta_{ij}(\mathbf{w}) = \zeta(\mathbf{w})\delta_{ij}$ for some $\zeta : \mathbb{R}^D \to \mathbb{R}$, then the result of the proposition reduces to $\frac{\partial}{\partial \mathbf{u}} d^C(\mathbf{w}, \mathbf{u})\big|_{\mathbf{u}=\mathbf{q}} = \sqrt{\zeta(\mathbf{q})}\ \mathbf{z}^T_{\mathbf{wq}}$ (where, $\mathbf{z}^T_{\mathbf{wq}} = [z^1_{\mathbf{wq}}, z^2_{\mathbf{wq}}, \cdots, z^D_{\mathbf{wq}}]$ is the transpose of the coefficient vector, $\mathbf{z_{wq}}$, of the tangent to the geodesic).

3. Finally, we consider a simple, yet nontrivial, example of a non-Euclidean, anisotropic metric. Consider this matrix representation of the metric tensor: $\eta_{\bullet\bullet} = \begin{bmatrix} 1 & 0 \\ 0 & 4 \end{bmatrix}$ (in coordinate chart C). Since the Christoffel symbols vanish in this coordinate chart, one can infer from the geodesic equation that the geodesics are essentially represented by straight lines when plotted with u^i as orthogonal axes (Figure 7(b)). However, the curves of constant distance from $\mathbf{w}$ become ellipses centered at $\mathbf{w}$ and with aspect ratio of 2. Now consider the point $\mathbf{q} = \mathbf{w} + [1, 1]^T$. A direct computation of the normal at this point to the ellipse, $(u^1 - w^1)^2/4 + (u^2 - w^2)^2 = c$, passing through this point, reveals the coefficient co-vector of $\frac{\partial}{\partial \mathbf{u}} d^C(\mathbf{w}, \mathbf{u})\big|_{\mathbf{u}=\mathbf{q}}$ to be parallel to $[\frac{1}{2}, 2]$. However, the coefficient vector of the tangent to

the geodesic is $\mathbf{z_{wq}} = [\frac{1}{\sqrt{2}}, \frac{1}{\sqrt{2}}]^T$. This gives the following: $\sqrt{\eta_{mn}(\mathbf{q})\, z^m_{\mathbf{wq}} z^n_{\mathbf{wq}}} = \sqrt{\frac{5}{2}}$, $z_{1,\mathbf{wq}} = \sum_j \eta_{1j}\, z^j_{\mathbf{wq}} = \frac{1}{\sqrt{2}}$, $z_{2,\mathbf{wq}} = \sum_j \eta_{2j}\, z^j_{\mathbf{wq}} = 2\sqrt{2}$. Thus, the coefficient co-vector of $\mathbf{z^*_{wq}}$ is parallel to $[\frac{1}{\sqrt{2}}, 2\sqrt{2}]$. This indeed is parallel to $[\frac{1}{2}, 2]$. The exact computation of the scalar multiple will require a more careful computation of $\frac{\partial}{\partial \mathbf{u}} d^C(\mathbf{w}, \mathbf{u})$.

In the following corollary we relax some conditions imposed on U in the Lemma L4 so that we can generalize the result to manifolds that are not necessarily geodesically convex.

Corollary C1. *Let Ω be a N-dimensional manifold possibly with boundaries, which is complete as a metric space, with length metric d_ℓ. Let $p \in \Omega$ and $q \in \Omega - (p \cup \partial\Omega \cup \mathcal{C}_p)$. Let q be such that the metric in its neighborhood is induced by a Riemannian metric tensor, η. Let d_ℓ be the length metric on Ω.*

Then the following holds for every coordinate chart, $D = (V, \psi)$, defined on open set $V \ni q$,

$$\left[\frac{\partial}{\partial \mathbf{u}} d^{\tilde{D}}_\ell(p, \mathbf{u})\Big|_{\mathbf{u}=\mathbf{q}}\right]_i \equiv \frac{\partial}{\partial u^i} d^{\tilde{D}}_\ell(p, \mathbf{u})\Big|_{\mathbf{u}=\mathbf{q}} = \frac{\eta_{ij}(\mathbf{q})\, z^j_{p\mathbf{q}}}{\sqrt{\eta_{mn}(\mathbf{q})\, z^m_{p\mathbf{q}} z^n_{p\mathbf{q}}}}$$

where, $\mathbf{q} = \psi(q)$, and $\mathbf{z}_{p\mathbf{q}} = [z^1_{p\mathbf{q}}, z^2_{p\mathbf{q}}, \cdots, z^D_{p\mathbf{q}}]^T$ is the coefficient vector (in coordinate chart D) of the tangent vector at q to the shortest geodesic connecting $p \in \Omega$ to $q \in V$. By $\left[\frac{\partial f}{\partial \mathbf{u}}\right]_i$ we mean the i^{th} component of $\left[\frac{\partial f}{\partial u^1}, \frac{\partial f}{\partial u^2}, \cdots, \frac{\partial f}{\partial u^D}\right]$.

Remark R4. This Corollary is applicable to a wider class of metric spaces than Lemma L4. Here we only need to assume a Riemannian metric in the neighborhood of q (Figure 8(a)). This will enable us to use the result for *locally* Riemannian manifolds allowing for pathologies outside local neighborhoods (*e.g.* boundaries/holes/punctures/obstacles – the kind of spaces we are most interested in), as well as opens up possibilities for more general metric spaces that may not be Riemannian outside a small ball neighborhood of q, $\mathcal{B}_q$ (e.g. Manhattan metric in $\mathcal{M} \subset \Omega$, Riemannian metric elsewhere). However, in this paper we will not consider the later kind of cases.

Examples:

1. The simplest example of a space that is only locally Euclidean is one that is $\mathbb{R}^2$ punctured by polygonal obstacles (Figure 8(b)). Due to the 'pointedness' of the obstacles, the constant-g_p manifolds are essentially circular arcs centered at p or a vertex v of a polygon. Thus, as illustrated by Figure 8(b), the normals to the arcs are parallel to the tangent to the segment joining v to q.

2. A less trivial case is seen in the example where the obstacles have curved boundaries. Then the corollary essentially reduces to the assertion that the normal at any point on an involute [Cundy 89] is parallel to the 'taut string', the end of which traces the involute – and this is true irrespective of the curve used to generate the involute. While the statement has an obvious intuitive explanation by considering the possible directions of motion of the end of the taut string, we provide an explicit computation for an involute created using a circle (Figure 8(c)). Consider a taut string unwrapping off a circle of radius r (starting from $\theta = 0$ when it is completely wrapped). Thus, when the string has unwrapped by an angle θ, the string

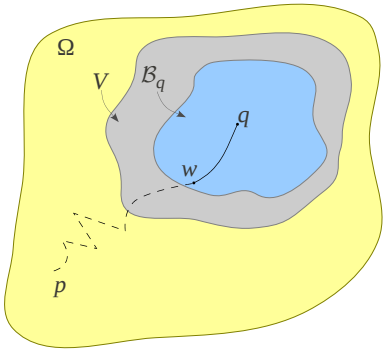

(a) Illustration for Corollary C1. The pathologies outside $\mathcal{B}_q$ do not effect the result of Lemma L4 holding for p and q.

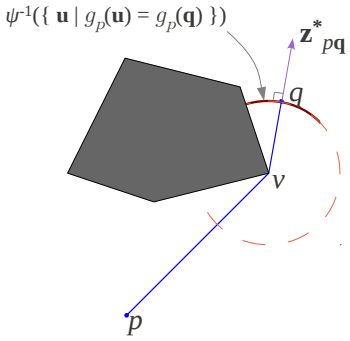

(b) Example of a space that is equipped with Euclidean metric everywhere, but is punctured by a polygonal obstacles. Here the $g_p(q) = const.$ curve consists of circular arcs. This was the case considered in [Pimenta 08].

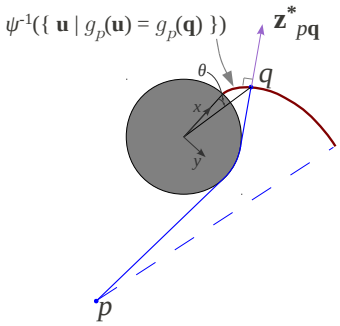

(c) An example with a circular obstacle where the $g_p(q) = const.$ curve consists of an involute and circular arc.

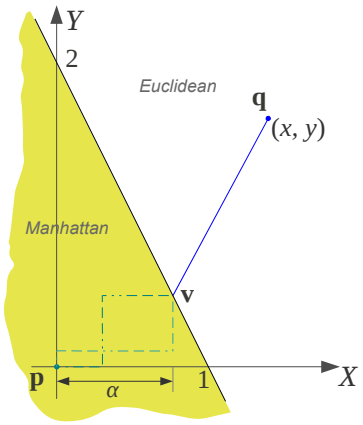

(d) An example involving Manhattan and Euclidean metrics in two different regions. The distance function between points lying in the two different regions is given by $d(\mathbf{p}, \mathbf{q}) = \min_{\mathbf{v}} (d_{man}(\mathbf{p}, \mathbf{v}) + d_{eu}(\mathbf{v}, \mathbf{q}))$, where $\mathbf{v}$ is a point lying on the boundary of the two regions.

Figure 8: Corollary C1 and illustrative examples.

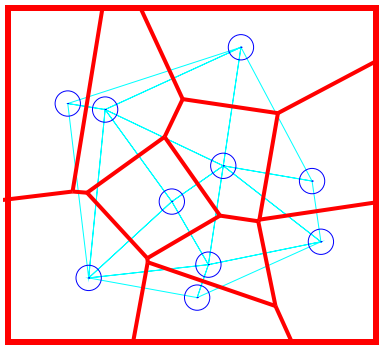

Figure 9: Voronoi tessellation of a convex Ω (rectangular region) with $n = 10$ robots (blue circles). The red line segments show the boundary of the tessellation. Note how a boundary segment is the perpendicular bisector of the cyan line joining the robots sharing the boundary segment.

points at a direction $[\sin(\theta), -\cos(\theta)]^T$. Now, it is easy to verify that the involute is described by the parametric curve $x = r(\cos(\theta) + \theta\sin(\theta)), y = r(\sin(\theta) - \theta\cos(\theta))$. Thus we have $\frac{\mathrm{d}x}{\mathrm{d}\theta} = \theta\cos(\theta)$, $\frac{\mathrm{d}y}{\mathrm{d}\theta} = \theta\sin(\theta)$. Thus the normal to the involute pointing in the direction $[\frac{\mathrm{d}y}{\mathrm{d}\theta}, -\frac{\mathrm{d}x}{\mathrm{d}\theta}]$ is indeed parallel to the direction in which the string points.

3. The last example that we will illustrate involves a mixture of Manhattan distance (in a particular given coordinate chart) and Euclidean metric. Consider the case in Figure 8(d), where in the given coordinate chart $\mathbf{p}$ is the origin, $(0, 0)$. For any two points inside the half-plane $\mathcal{M} = \{(x, y)|2x + y < 2\}$, the distance function is the Manhattan distance. Outside $\mathcal{M}$ it is induced by Euclidean metric. It is to be noted that although the distance function is defined in $\mathcal{M}$, geodesics are not uniquely defined. Let us consider the point $\mathbf{q} = (x, y)$ outside $\mathcal{M}$ (so that there exists a $\mathcal{B}_\mathbf{q}$ as required by Corollary C1). The distance is given by $d(\mathbf{p}, \mathbf{q}) = \min_{\alpha\in\mathbb{R}} \left(\alpha + 2(1-\alpha) + \sqrt{(x-\alpha)^2 + (y-2(1-\alpha))^2}\right)$. Denoting the quantity inside 'min' by $f(\alpha)$, and by solving $\frac{\partial f}{\partial \alpha} = 0$, one obtains the unique solution $\alpha = (4x - 3y + 6)/10$. This gives $d(\mathbf{p}, \mathbf{q}) = (3x + 4y + 12)/5$. Thus, the normals to the constant-d surfaces are parallel to $[3/5, 4/5]$. Again, the segments $\overline{\mathbf{vq}}$ have tangent pointing in the direction $[x - \alpha, y - 2(1-\alpha)]^T = [(6x + 3y - 6)/10, (8x + 4y - 8)/10]^T$. Thus we see that they are indeed parallel.

3 The coverage problem in robotics

Background: In this section we discuss the derivation of the control laws in the continuous-time version of the Lloyd's algorithm. We start with the classical case for convex environments with Euclidean metric [Lloyd 82], and from that motivate our generalization to general manifolds with boundary and general Riemannian metric.

Let Ω be a path-connected metric space that represents the environment, equipped with a metric, $d_* : \Omega \times \Omega \to \mathbb{R}_+$. In [Lloyd 82, Pimenta 08] Ω is assumed to be a convex subset of $\mathbb{R}^N$ and is equipped with the Euclidean metric tensor at every point. However, in the present scenario we relax d_* to a more general metric on a metric space, Ω, that need not necessarily be a manifold. We will eventually consider the length metric, d_ℓ, on manifolds with boundary, induced by a general Riemannian metric. We will introduce those restrictions gradually as they are required.

Coverage functional: Suppose there are n mobile robots in Ω. The position of the k^{th} robot is represented by $p_k \in \Omega$. By definition, a *tessellation* [Lloyd 82, Pimenta 08] of the environment is a partition of Ω, written as $\{W_k\}_{k=1,2,\cdots,n}$, such that each W_k (called a *tessella*) is path connected, $p_k \in W_k$, $Int(W_k) \cap Int(W_l) = \emptyset, \forall k \neq l$, and $\cup_{k=1}^{n} W_k = \Omega$. The *tessella* associated with the k^{th} robot is $W_k, \forall k = 1, 2, \ldots, n$. For a given set of robot positions $P = \{p_1, p_2, \ldots, p_n\}$ and tessellation $W = \{W_1, W_2, \ldots, W_n\}$, the *coverage functional* is defined as:

$$\mathcal{H}(P, W) = \sum_{k=1}^{n} \mathcal{H}(p_k, W_k) = \sum_{k=1}^{n} \int_{W_k} f_k(d_*(q, p_k))\, w(q)\, \mathrm{d}q \tag{1}$$

where $f_k : \mathbb{R}_+ \to \mathbb{R}$ are smooth and strictly increasing functions, $w : \Omega \to \mathbb{R}_+$ is a weight or density function, and $\mathrm{d}q$ represents an infinitesimal volume element (more formally, it is a top-dimensional *measure* of an an infinitesimal element, associated with the metric d_* [Gromov 99]).

The name "*coverage functional*" is indicative of the fact that $\mathcal{H}$ measures how *bad* the coverage is — *i.e.*, more well-distributed the robots are throughout the environment, lower is the value of $\mathcal{H}$. In fact, for a given set of initial robot positions, P, we devise a control law that minimizes the function $\tilde{\mathcal{H}}(P) := \min_{W} \mathcal{H}(P, W)$ (*i.e.* the best value of $\mathcal{H}(P, W)$ for a given P). It is easy to show [Lloyd 82, Pimenta 08] that $\tilde{\mathcal{H}}(P) = \mathcal{H}(P, V)$, where $V = \{V_1, V_2, \cdots, V_n\}$ is the Voronoi tessellation given by

$$V_k = \{q \in \Omega \mid f_k(d_*(q, p_k)) \leq f_l(d_*(q, p_l)), \forall l \neq k\} \tag{2}$$

Requiring Ω to be a manifold with boundary: The control law for minimizing $\tilde{\mathcal{H}}(P) = \sum_{k=1}^{n} \int_{V_k} f_k(d_*(q, p_k)) w(q)\, \mathrm{d}q$ can be reduced to the problem of moving along the direction of its steepest descent. So far in this section we have not required that Ω be a manifold. However, we would like to be able to compute the gradient of $\tilde{\mathcal{H}}(P)$ so that the negative of it is the direction of steepest descent. It suffices that the configuration space be a manifold so that each point on it has a tangent space in which the gradient of a function (or its negative) will reside. However, based on our discussions in Section 2, we are now capable of defining and computing gradients on manifolds with boundary (see Remark *R3*). However, we need to check the existence of the negative of the gradient inside the *tangent cone* at a point on the boundary, so that the robots can move along that direction. In the following discussion we use explicit coordinate charts, $C_k = (U_k, \phi_k)$, with $p_k \in U_k$ — the position of the k^{th} robot, at which we compute the gradients. Using the notation introduced in Corollary C1, we write $d_*^{\tilde{C}_k}(a, \mathbf{b}) := d_*(a, \phi_k^{-1}(\mathbf{b}))$ for $\mathbf{b} \in Img(\phi_k)$.

The domains of integration, V_k are functions of P, and hence the gradient of $\tilde{\mathcal{H}}(P)$ would, in general, involve boundary terms, ∂V_k. However, it can be shown using methods of differentiation under integration [Pimenta 08] that the boundary terms vanish. So the final formula for the partial derivatives of $\tilde{\mathcal{H}}(P)$ with respect to the position of the robots become,

$$\frac{\partial \tilde{\mathcal{H}}(P)}{\partial \mathbf{p}_k} = \int_{V_k} \frac{\partial}{\partial \mathbf{p}_k} f_k(d_*^{\tilde{C}_k}(q, \mathbf{p}_k))\, w(q)\, \mathrm{d}q \tag{3}$$

In practice, it is adequate to choose $f_k(x) = x^2$ for most implementations [Cortes 04]. However, a variation of the problem for taking into account finite sensor footprint of the robots, constructs a *power Voronoi tessellation* [Pimenta 08], in which one chooses $f_k(x) = x^2 - R_k^2$, where R_k can represent, for example, the radius of the sensor footprint of the k^{th} robot. In this paper we will be working with the following form for f_k

$$f_k(x) = x^2 + c_k \tag{4}$$

Requiring d_* to be a metric induced by Riemannian metric tensor: Until now we haven't made any major assumption on the distance function d_* besides the fact that it is a metric on a manifold with boundaries that can be differentiated at the points p_k. We next impose the condition that the metric is locally represented by a Riemannian metric tensor, η.

> *Remark R5.* If the space Ω is convex, and we can construct a single coordinate chart, $B = \{\Omega, \psi\}$, over entire Ω such that the matrix representation of the metric tensor is Euclidean everywhere, then d_* is the Euclidean distance given by $d_*^B(\mathbf{x}, \mathbf{y}) = \|\mathbf{x} - \mathbf{y}\|_2$ (where, $d_*^B(\mathbf{a}, \mathbf{b}) = d_*(\psi^{-1}(\mathbf{a}), \psi^{-1}(\mathbf{b}))$ – refer to notation introduced in Lemma L4). This was the case considered in [Lloyd 82] (see Figure 9). Under this assumption, and using the form of f_k in (4), the formula of (3) can be simplified to obtain
>
> $$\frac{\partial \tilde{\mathcal{H}}(P)}{\partial \mathbf{p}_k} = 2A_k(\mathbf{p}_k - \mathbf{p}_k^*) \tag{5}$$
>
> where, $A_k = \int_{V_k} w(q)\ \mathrm{d}q$ is the weighted *volume* of V_k, and $\mathbf{p}_k^* = \frac{\int_{V_k} \mathbf{q}\ w(q)\ \mathrm{d}q}{A_k}$ (with $\mathbf{q} = \psi(q)$, the coordinate representation of q) is the *weighted centroid* of V_k. Moreover, the Euclidean distance function makes computation of the Voronoi tessellation very easy: V, due to Equation (2), can be constructed from the *perpendicular bisectors* of the line segments $\overline{\mathbf{p}_k\mathbf{p}_l}$, $\forall k \neq l$ in the coordinate chart B, thus making each V_k a convex polygon, which are also simply connected (Figure 9). This also enable closed-form computation of the volume, A_k, and the centroid, $\mathbf{p}_k^*$ when the weight function, w, is uniform. Equation (5) yields the simple control law (in coordinate chart B) in continuous-time Lloyd's algorithm: $\mathbf{u}_k = -\kappa A_k(\mathbf{p}_k - \mathbf{p}_k^*)$, with some positive *gain*, κ. Lloyd's algorithm [Lloyd 82] and its continuous-time asynchronous implementations [Cortes 04] are distributed algorithms for minimizing $\mathcal{H}(P, W)$ with guarantees on completeness and asymptotic convergence to a local optimum, when Ω is convex Euclidean. However, this simplification does not work when there does not exist a coordinate chart as B in which the metric can be expressed as the Euclidean norm of difference for every pair of points — an inherent characteristic of spaces with holes/obstacles or with metric that is intrinsically non-Euclidean.

Requiring d_* to be the length metric: We also impose the condition that the metric be the length metric, *i.e.* $d_* = d_\ell$, that was introduced in Section 2.2. In the following discussion we will hence use results derived in Section 2 to make assertions about the existence of the gradient, and hence the convergence.

Now, with $f_k(x) = x^2 + c_k$, we have $\frac{\partial}{\partial \mathbf{p}_k} f_k(d_\ell^{\tilde{C}_k}(q, \mathbf{p}_k)) = 2\ d_\ell(q, p_k)\ \frac{\partial}{\partial \mathbf{p}_k} d_\ell^{\tilde{C}_k}(q, \mathbf{p}_k)$ where, $\mathbf{p}_k = \phi_k(p_k)$. Substituting this into Equation (3) and using Proposition P1 (with the explicit formula from Corollary C1) we obtain,

$$\begin{aligned}
\left[\frac{\partial \tilde{\mathcal{H}}(P)}{\partial \mathbf{p}_k}\right]_i &= 2\int_{V_k} d_\ell(q, p_k)\ \frac{\partial}{\partial \mathbf{p}_k} d_\ell^{\tilde{C}_k}(q, \mathbf{p}_k)\ \ w(q)\ \ \mathrm{d}q \\
&= 2\int_{V_k - (p \cup \mathcal{C}_{p_k})} d_\ell(q, p_k)\ \frac{\eta_{ij}(\mathbf{p}_k)\ z^j_{q\mathbf{p}_k}}{\sqrt{\eta_{mn}(\mathbf{p}_k)\ z^m_{q\mathbf{p}_k} z^n_{q\mathbf{p}_k}}}\ \ w(q)\ \ \mathrm{d}q
\end{aligned} \tag{6}$$

where $z^j_{q\mathbf{p}_k}$ is the j^{th} component of the coefficient vector (in coordinate chart C_k) of the tangent at p_k to the minimal path connecting q and p_k.

That we can write the second equality is due to the fact that $p_k \cup \mathcal{C}_{p_k}$ is a set of measure zero in V_k (a consequence of Lemma L2), outside which $\frac{\partial}{\partial \mathbf{p}_k} d_\ell^{\tilde{C}_k}(\cdot, \mathbf{p}_k)$ exists (a consequence of Proposition P1

and and Lemma L3): The domain of integration in the second integral implies $q \notin \mathcal{C}_{p_k}$. This, due to Lemma L3, implies that $p_k \notin \mathcal{C}_q$ almost always (*i.e.* for all p_k, except possibly for a set a measure zero in Ω). Also, $p_k \neq q$. This, due to Proposition P1, implies the gradient of $d_\ell(q,\cdot)$ exists at p_k. Thus we could write the quantity inside the second integral. Moreover, due to part 'i' of Lemma L2, $p_k \cup \mathcal{C}_{p_k}$ is a set of measure zero in V_k (since V_k is not a set of measure zero in Ω). Also, due to part 'iii.' of the same lemma, the gradient at the points in the neighborhoods of $p_k \cup \mathcal{C}_{p_k}$ is finite. Thus, removing $p_k \cup \mathcal{C}_{p_k}$ from the domain of integration does not change the value of the integral, but lets us compute the integral.

We consider the negative of the quantity in (6). The $\left[-\frac{\partial \tilde{\mathcal{H}}(P)}{\partial \mathbf{p}_k}\right]_i$ are coefficients (in chart C_k) of a covector that resides in $T^*_{p_k}\Omega$. The corresponding vector (the dual) will thus have coefficients $\left[-\frac{\partial \tilde{\mathcal{H}}(P)}{\partial \mathbf{p}_k}\right]_i \eta^{il}(\mathbf{p}_k)$ (where $\eta^{\bullet\bullet}$ is matrix inverse of the matrix representation of the metric tensor, $\eta_{\bullet\bullet}$ [Jost 97, Petersen 06]). This is the vector along which the k^{th} robot needs to be moved for reducing the value of $\tilde{\mathcal{H}}$ the most. Using a scalar gain of κ and noting that $\eta_{ij}\eta^{il} = \delta^l_i$, the l^{th} coefficients of the control vector for the k^{th} robot will be

$$\begin{aligned}
[\mathbf{u}_k]^l \;=:\; u^l_k \;&=\; \kappa \left[-\frac{\partial \tilde{\mathcal{H}}(P)}{\partial \mathbf{p}_k}\right]_i \eta^{il}(\mathbf{p}_k) \\
&=\; 2\,\kappa \int_{V_k - (p \cup \mathcal{C}_{p_k})} d_\ell(q,p_k)\, \frac{-z^j_{q\mathbf{p}_k}}{\sqrt{\eta_{mn}(\mathbf{p}_k)\; z^m_{q\mathbf{p}_k} z^n_{q\mathbf{p}_k}}}\; w(q)\;\; \mathrm{d}q
\end{aligned} \tag{7}$$

We now test if this vector actually exists in $T_{p_k}\Omega$ for all p_k (including ones on $\partial\Omega$). Clearly $-z^j_{q\mathbf{p}_k}\frac{\partial}{\partial x^j}$ exists in $T_{p_k}\Omega$, since the minimal path connecting p_k and q exists (see proof of Proposition P1). Now we recall that $T_{p_k}\Omega$ is a convex cone almost everywhere in Ω due to Lemma L1 and Remark *R1* (except for possibly isolated points on $\partial\Omega$, in which case we either smoothen the boundary near that point or rely on presence of small noise that would 'push' the robot out that isolated point – see Remark *R2*). Thus a positive linear combination of vectors in $T_{p_k}\Omega$ (which the quantity in (7) is) will also be in $T_{p_k}\Omega$. This essentially implies that if the k^{th} robot follows this control law, it won't get 'stuck' at a point on the boundary. It will stop only when the gradient of $\tilde{\mathcal{H}}$ becomes zero, making the control vector zero.

As discussed earlier, a single coordinate chart over entire Ω may not exists. However, for many computational purposes, one can use a single coordinate chart, $B = (\Omega\text{–}\mathcal{S}, \psi)$, that describes almost the whole of Ω, except for a set of measure zero, $\mathcal{S}$ (*e.g.* the polar coordinate on a sphere describes everything except one longitudinal line and the poles). Thus, it is worth re-writing equation (7) entirely in terms of a coordinate chart. Besides changing q to $\mathbf{q} = \psi(q)$ and p_k to $\mathbf{p}_k = \psi(p_k)$, we need to compute the volume of the infinitesimal element $\mathrm{d}q$ in the particular coordinate chart. Assuming $\mathrm{d}\mathbf{q}$ to be an infinitesimal element in a particular coordinate chart, this is given by $\mathrm{d}q = \sqrt{\det(\eta_{\bullet\bullet}(\mathbf{q}))}\,\mathrm{d}\mathbf{q}$. Thus we have,

$$u^l_k \;=\; 2\kappa \int_{V_k - (p \cup \mathcal{C}_{p_k} \cup \mathcal{S})} d^B_\ell(\mathbf{q},\mathbf{p}_k)\, \frac{-z^j_{\mathbf{qp}_k}}{\sqrt{\eta_{mn}(\mathbf{p}_k)\; z^m_{\mathbf{qp}_k} z^n_{\mathbf{qp}_k}}}\; w^B(\mathbf{q})\;\sqrt{\det(\eta_{\bullet\bullet}(\mathbf{q}))}\,\mathrm{d}\mathbf{q} \tag{8}$$

where d^B_ℓ is the length metric expressed in terms of coordinate chart B, *i.e.*, $d^B_\ell(\mathbf{a},\mathbf{b}) = d_\ell(\psi^{-1}(\mathbf{a}), \psi^{-1}(\mathbf{b}))$. Likewise, $w^B : \mathbb{R}^N \to \mathbb{R}_+$ such that $w^B(\mathbf{a}) = w(\psi^{-1}(\mathbf{a}))$. $\mathbf{z}_{\mathbf{qp}_k} = [z^1_{\mathbf{qp}_k}, z^2_{\mathbf{qp}_k}, \cdots, z^D_{\mathbf{qp}_k}]^T$ is the coefficient vector (in chart B) of the tangent vector at q to the minimal path joining p_k and q. We emphasize on the fact that $(p \cup \mathcal{C}_{p_k} \cup \mathcal{S})$ is a set of measure zero in Ω, and does not concern us as far as computation is concerned.

The formula in (8), as we will see in the next section, gives an algorithm for approximately computing the gradient of $\tilde{\mathcal{H}}$. This give a generalized Lloyd's algorithm with guarantee of asymptotic stability (since we showed that the control vector will always exist in the tangent cones at points in Ω, and hence the only way the robots can stop is when the control becomes zero, *i.e.* the gradient of $\tilde{\mathcal{H}}$ vanishes). In the final converged solution, each robot will be at the *generalized centroid* of its related Voronoi tessellation.

4 Graph Search-based Implementation

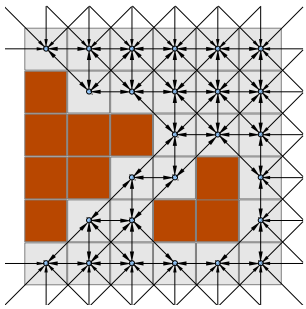

Figure 10: Graph construction: An 8-connected grid graph created from a uniformly discretized coordinate space. The brown cells represent obstacles.

In order to develop a version of the generalized continuous-time Lloyd's algorithm for a general distance function, we first need to be able to compute the general Voronoi tessellation of Equation (2) for the metric, d_ℓ. We adopt a discrete graph-search based approach for achieving that, not unlike the approach taken in previous work [Bhattacharya 10]. We consider a uniform square tiling (Figure 10) of the space of coordinate variables (in a particular coordinate chart) and create a graph G out of it (with vertex set $\mathcal{V}(G)$, edge set $\mathcal{E}(G) \subseteq \mathcal{V}(G) \times \mathcal{V}(G)$ and cost function $\mathcal{C}_G : \mathcal{E}(G) \to \mathbb{R}_+$). The costs/weights of the edges of the graph are the metric lengths of the edges. It is to be noted that in doing so we end up restricting the metric of the original space to the discrete graph. Because of this, as well as due to the discrete computation of the integrations (as discussed later), this discrete graph-search based approach is inherently an approximate method, where we trade off the accuracy and elegance of a continuous space for efficiency and computability with arbitrary metric.

The key idea is to make a basic modification to Dijkstra's algorithm [Dijkstra 59, Cormen 01]. This enables us to create a geodesic Voronoi tessellation. For creating Voronoi tessellation we initiate the *open set* with multiple start nodes from which we start propagation of the wavefronts. Thus the wavefronts emanate from multiple sources. The places where the wavefronts collide will hence represent the boundaries of the Voronoi tessellation. In addition, we can conveniently alter the distance function, the level-set of which represents the boundaries of the Voronoi tessellation. This enables us to even create *geodesic power Voronoi tessellation*. Figure 11 illustrates the progress of the algorithm in creation of the tessellation.

In order to compute the control command for the robots (*i.e.* the action of the robot in the next time step), we use the formula in Equation (8). In a discretized setup, the position of the k^{th} robot corresponds to a vertex $\mathrm{p}_k \in \mathcal{V}(G)$ (note that we use a vertical, regular-weight font to distinguish a vertex from the point $p_k \in \Omega$ or its coordinate representation $\mathbf{p}_k$). The coefficient vector $\mathbf{z}_{\mathbf{q}\mathbf{p}_k}$ of the

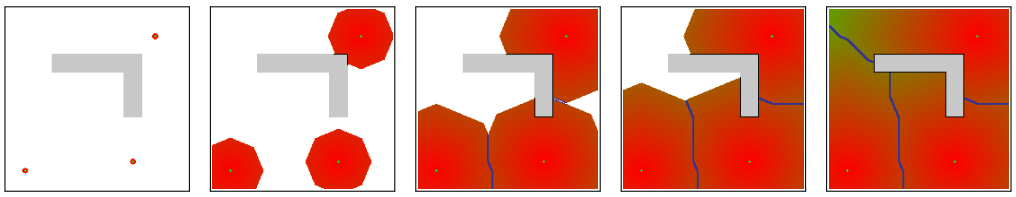

(a) $iter = 1$. (b) $iter = 10100$. (c) $iter = 25100$. (d) $iter = 30100$. (e) $iter = 37300$.

Figure 11: Progress of the algorithm for tessellation and control computation in an environment with a L-shaped obstacle. The graph is constructed by 200×200 uniform square discretization of the environment (see [Bhattacharya 10]). Tessellation is created starting from three points (the location of the agents) to the complete diagram after expansion of about 37300 vertices. The filled area indicates the set of *expanded* vertices. The boundaries of the tessellation are visible in blue.

tangent vector is approximated by the coefficient vectors along edges of the form $[\mathrm{p}'_k, \mathrm{p}_k] \in \mathcal{E}(G)$ for some $\mathrm{p}'_k \in \mathcal{N}_G(\mathrm{p}_k)$ (the set of neighbors of p_k) such that the shortest path in the graph connecting p_k and $\mathrm{q} \in \mathcal{V}(G)$ passes through p'_k. For a given q, we know the index of the robot, $\tau(\mathrm{q})$, whose tessella it belongs to, and can compute the shortest path in the graph joining the vertices $\mathrm{p}_{\tau(\mathrm{q})}$ and q. The neighbor of $\mathrm{p}_{\tau(\mathrm{q})}$, through which the shortest path passes, is the desired $\mathrm{p}'_{\tau(\mathrm{q})}$, and it is maintained in a variable $\eta(\mathrm{q})$ in an efficient way. Thus, we can also compute the integration of (8) on the fly (by approximating it as a summation over the discrete cells) as we compute the tessellation. The complete pseudo-code of the algorithm is given below.

$\{\tau, \{\mathrm{p}'_k\}\}$ = **Tessellation_and_Control_Computation** $(G, \{\mathrm{p}_k\}, \{R_k\}, \overline{w})$
Inputs: a. Graph G (with vertex set $\mathcal{V}(G)$, edge set $\mathcal{E}(G) \subseteq \mathcal{V}(G) \times \mathcal{V}(G)$, and cost function $\mathcal{C}_G : \mathcal{E}(G) \to \mathbb{R}_+$)
b. Agent locations $\mathrm{p}_k \in \mathcal{V}(G),\ k = 1, 2, \cdots, n$
c. Agent weight $R_k \in \mathbb{R}^+,\ k = 1, 2, \cdots, N$
d. Discretized weight/density function $\overline{w} : \mathcal{V}(G) \to \mathbb{R}$
e. The matrix representation of metric tensor, $\eta_{..} : Img(\psi) \to \mathbb{R}^{D \times D}$, in coordinate chart B
Outputs: a. The tessellation map $\tau : \mathcal{V}(G) \to \{1, 2, \cdots, n\}$
b. The next position of each robot, $\mathrm{p}'_k \in \mathcal{N}_G(\mathrm{p}_k),\ k = 1, 2, \cdots, n$

Initiate g: Set $g(\mathrm{v}) := \infty$, for all $\mathrm{v} \in \mathcal{V}(G)$ // Shortest distances
Initiate ρ: Set $\rho(\mathrm{v}) := \infty,\ \forall \mathrm{v} \in \mathcal{V}(G)$ // Power distances
Initiate τ: Set $\tau(\mathrm{v}) := -1,\ \forall \mathrm{v} \in \mathcal{V}(G)$ // Tessellation
Initiate ν: Set $\nu(\mathrm{v}) := \emptyset,\ \forall \mathrm{v} \in \mathcal{V}(G)$ // Pointer to robot neighbor. $\nu : \mathcal{V}(G) \to \mathcal{V}(G)$
for each $(\{k \in \{1, 2, \cdots, n\}\})$
    Set $g(\mathrm{p}_k) = 0$
    Set $\rho(\mathrm{p}_k) = -R_k^2$
    Set $\tau(\mathrm{p}_k) = k$
    Set $\mathbf{I}_k := \mathbf{0}$ // The negative of differential of $\tilde{\mathcal{H}}$ in coordinate chart B (a covector).
    for each $(\{\mathrm{q} \in \mathcal{N}_G(\mathrm{p}_k)\})$ // For each neighbor of p_k
        Set $\nu(\mathrm{q}) = \mathrm{q}$
Set $Q := \mathcal{V}(G)$ // Set of un-expanded nodes
while $(Q \neq \emptyset)$
    $\mathrm{q} := \mathrm{argmin}_{\mathrm{q}' \in Q}\ \rho(\mathrm{q}')$ // Maintained by a heap data-structure.
    if $(g(\mathrm{q}) == \infty)$
        break
    Set $Q = Q - \mathrm{q}$ // Remove q from Q

18 Set $l := \tau(\mathrm{q})$
19 Set $\mathrm{s} := \nu(\mathrm{q})$
20 **if** ($\mathrm{s} != \emptyset$) // Equivalently, $\mathrm{q} \notin \{\mathrm{p}_k\}_{k=1,2,\ldots,n}$
21 Set $\mathbf{z} = \mathbf{P}(\mathrm{s}) - \mathbf{P}(\mathrm{p}_l)$ // Negative of tangent vector
21 Set $\mathbf{M} = \eta_{\cdot\cdot}(\mathbf{P}(\mathrm{p}_l))$ // Metric tensor at p_l as a matrix in coordinate representation of B.
21 Set $\mathbf{I}_l \mathrel{+}= g(\mathrm{q}) \times \frac{\mathbf{Mz}}{\sqrt{\mathbf{z}^T\mathbf{Mz}}} \times \overline{w}(\mathrm{q}) \times \sqrt{\det \mathbf{M}}$ // Negative of integral in gradient of $\tilde{\mathcal{H}}$
22 **for each** ($\{\mathrm{w} \in \mathcal{N}_G(\mathrm{q})\}$) // For each neighbor of q
23 Set $g' := g(\mathrm{q}) + \mathcal{C}_G([\mathrm{q}, \mathrm{w}])$
24 Set $\rho' := \mathbf{PowerDist}(g', R_l)$
25 **if** ($\rho' < \rho(\mathrm{w})$)
26 Set $g(\mathrm{w}) = g'$
27 Set $\rho(\mathrm{w}) = \rho'$
28 Set $\tau(\mathrm{w}) = l$
29 **if** ($\mathrm{s} != \emptyset$) // Equivalently, $\mathrm{q} \notin \{\mathrm{p}_k\}_{k=1,2,\cdots,n}$
30 Set $\nu(\mathrm{w}) = \mathrm{s}$
31 **for each** ($\{k \in \{1, 2, \cdots, n\}\}$)
32 Set $\mathrm{p}'_k := \mathrm{argmax}_{\mathrm{u} \in \mathcal{N}_G(\mathrm{p}_k)} \ (\mathbf{P}(\mathrm{u}) - \mathbf{P}(\mathrm{p}_k)) \cdot \mathbf{I}_k$ // Choose action best aligned along $\mathbf{I}_k$.
33 **return** $\{\tau, \{\mathrm{p}'_k\}\}$

where, we used the coordinate chart $B = (\Omega - \mathcal{S}, \psi)$ as discussed earlier. The function $\mathbf{P} : \mathcal{V}(G) \to \Omega$ is such that $\mathbf{P}(\mathrm{q})$ gives the coordinate of the vertex q. Thus, $\mathbf{P}(\mathrm{p}_k) = \mathbf{p}_k$ and $\mathbf{P}(\mathrm{q}) = \mathbf{q}$ in relation to Equation (8). In an uniform discretization setting we take $\overline{w}(\mathrm{q}) = \alpha\ w(\psi^{-1}(\mathbf{P}(\mathrm{q})))$ for an arbitrary positive constant α representing the 'area' of each discretized cell. Note that $\mathbf{I}_k$ is the coefficient vector of the differential of $\tilde{\mathcal{H}}$ (a covector), while $\mathbf{u}_k$ is its dual (a vector – see Equation (7)). Thus, in line 32 of the algorithm, the 'dot product' is an element-wise product followed by a summation and not the inner product (*i.e.* for $a \in T_p^*\Omega$ and $b, c \in T_p\Omega$, we define $a \cdot b = a_i b^i$, but $<b, c>= \eta_{ij} b^i c^j$). The function $\mathbf{PowerDist}(x, R_k) \equiv f_k(x) = x^2 - R_k^2$ computes the *power distance* for *power Voronoi tessellation*.

The complexity of the algorithm is the same as the standard Dijkrstra's algorithm, which for a constant degree graph is $O(V_G \log(V_G))$ (where $V_G = |\mathcal{V}(G)|$ is the number of vertices in the graph). This is in sharp contrast to the complexity of search for optimal location as in [Durham 12].

4.1 Application to Coverage on Non-Euclidean Metric Spaces

In this section we will illustrate examples of coverage using the generalized continuous-time Lloyd's algorithm on a 2-sphere. We use a coordinate chart with coordinate variables $x \in (0, \pi)$, the latitudinal angle, and $y \in [0, 2\pi)$, the longitudinal angle (Figure 12(a)). The matrix representation of the metric on the sphere using this coordinate chart is $\eta_{\bullet\bullet} = \begin{bmatrix} 1 & 0 \\ 0 & \sin^2(x) \end{bmatrix}$. As usual, we use a uniform square discretization of the coordinate space to create an 8-connected grid graph [Bhattacharya 10]. However, in order to model the complete sphere (in the example of Figure 13), we need to establish appropriate edges between vertices at the extreme values of y, *i.e.* the ones near $y = 0$ and $y = 2\pi$. Similarly, we use an additional vertex for each pole to which the vertices corresponding to the extreme values of x connect.

Figure 12(b)-(d) shows two robots pursuing the coverage control law on a subset of the 2-sphere by following the control command computed using the algorithm of Section 4 at every time-step. The region of the sphere that we restrict to is that of latitudinal angle $x \in [\pi/16, 3\pi/4]$, and longitudinal angle $y \in [\pi/16, 3\pi/4]$. The robots start off from the bottom left of the environment near the point $[0.42, 0.45]$, and follow the control law of Equation (8) until convergence is achieved. Note

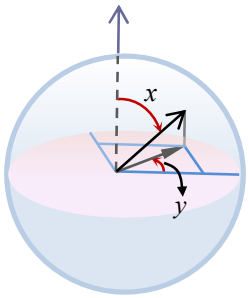

(a) The 2-sphere and a coordinate chart on it.

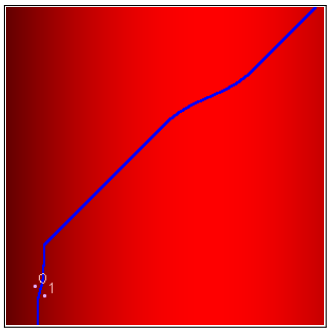

(b) $t = 1$.

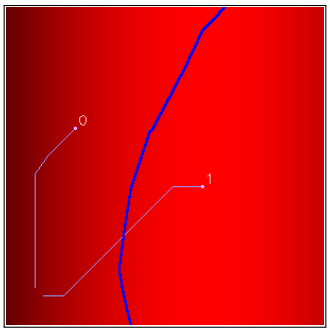

(c) $t = 150$.

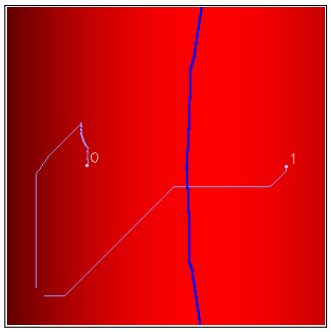

(d) $t = 250$. Converged solution.

Figure 12: Coverage using a discrete implementation of generalized continuous-time Lloyd's algorithm on a part of the 2-sphere. The chosen coordinate variables, x and y, are the latitudinal and longitudinal angles respectively, and the domain shown in figures (b)-(d) represent the region on the sphere where $x \in [\pi/16, 3\pi/4], y \in [\pi/16, 3\pi/4]$. x is plotted along horizontal axis and y along vertical axis on linear scales. The intensity of red indicates the determinant of the metric, the thick blue curves are the tessellation boundaries, and the thin pale blue curves are the robot trajectories.

that the tessellation has a curved boundary in Figures 12(c) and 12(d) because it has to be a segment of the great circle on the sphere (note that the jaggedness is due to the fact that the curve actually resides on the discrete graph rather than the original metric space of the sphere). In the converged solution of Figure 12(d), note how the robots get placed such that the tessellation splits up the area on the sphere equally rather than splitting up the area of the non-isometric embedding in $\mathbb{R}^2$ that depends on the chosen coordinate chart. The weight function is chosen to be constant, $w(q) = 1$. For this example, the program ran at a rate of about 4 Hz on a machine with 2.1 GHz processor and 3 Gb memory.

A more complete example is shown in Figure 13 in which 4 robots attain coverage on a complete 2-sphere. The robots start off close to each other on the sphere, and follow the control law of Equation (8), until they converge attaining good and uniform coverage of the sphere. In order to avoid numerical problems near the poles, we cordon off small disks near the poles (marked by the gray regions), and establish 'invisible' edges across those disks connecting the vertices on their diametrically opposite points. Figures 13(a)-(d) show the tessellation in the coordinate chart with x plotted along the horizontal axis and y along the vertical axis (300×600 uniformly discretized).

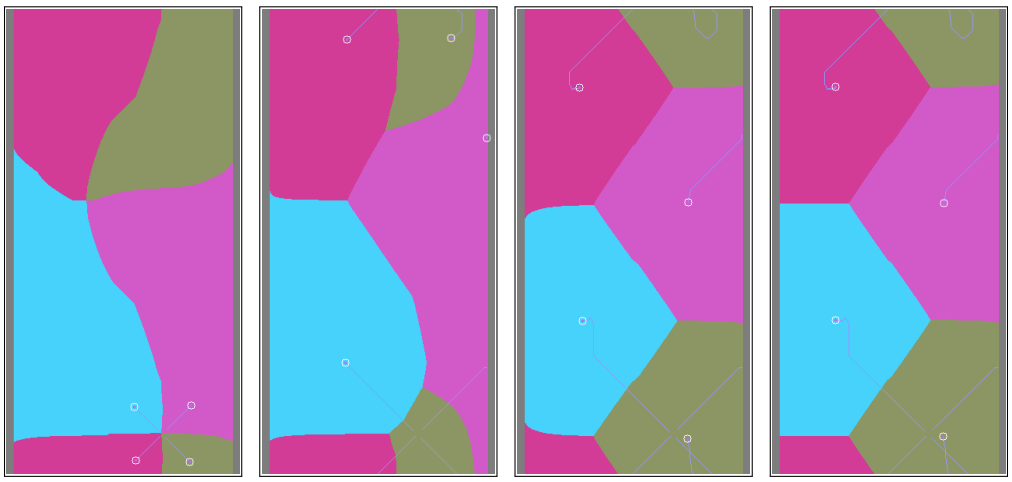

(a) $t = 32$. (b) $t = 88$. (c) $t = 171$. (d) $t = 211$.

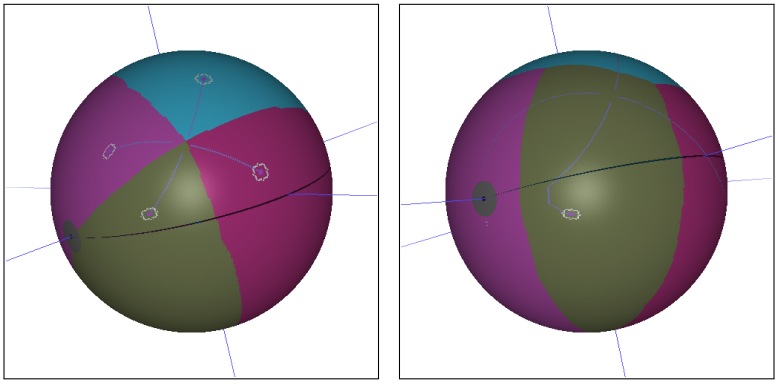

(e) $t = 32$. (f) $t = 88$.

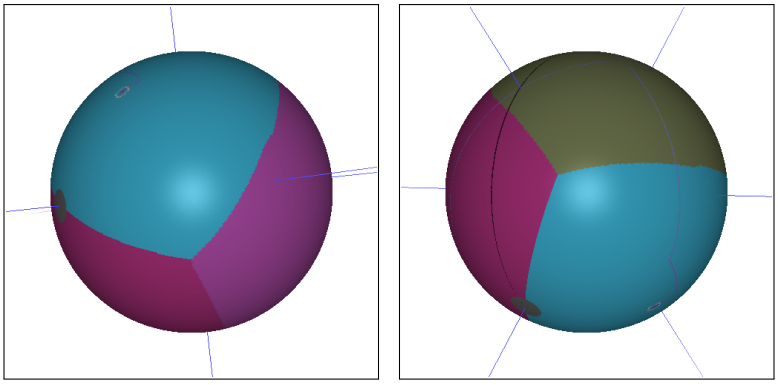

(g) $t = 171$. (h) $t = 211$.

Figure 13: Coverage on a complete sphere. In Figures (a)-(d), $x \in (0, \pi)$ (latitudinal angle) is plotted along horizontal axis and $y \in [0, 2\pi)$ (longitudinal angle) along vertical axis on linear scales. Figures (e)-(h) show the same plot mapped on the 2-sphere. The colors are used to indicate the tessella of the robots. Note that in (e)-(h) different viewing angles are used to facilitate visualization. (d) and (h) are the converged solutions. Also see Extension 1.

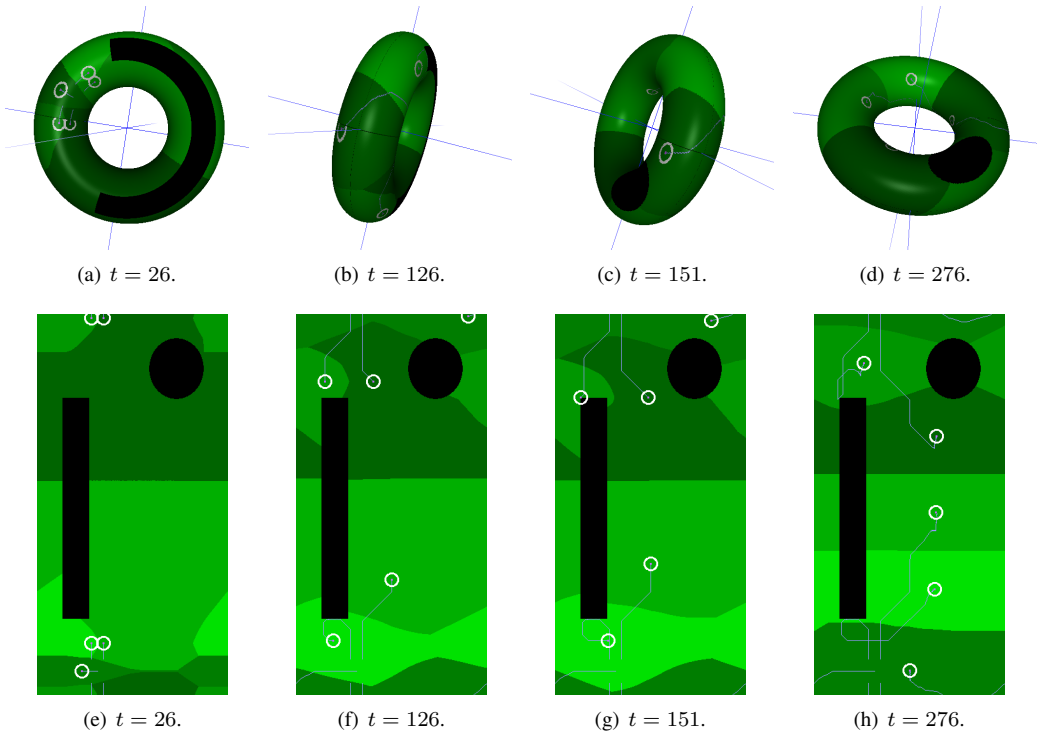

(a) $t = 26$. (b) $t = 126$. (c) $t = 151$. (d) $t = 276$.

(e) $t = 26$. (f) $t = 126$. (g) $t = 151$. (h) $t = 276$.

Figure 14: Coverage control on a 2-torus with two obstacles on it (marked in black) with 5 robots. (a)-(d): The torus is rotated to view from different angles as the coverage algorithm progresses. (e)-(h): The plot on the coordinate chart. Also see Extension 1.

Figures 13(e)-(h) show the same tessellation mapped on the sphere. The weight function, once again is chosen to be $w(q) = 1$. For this example, the program ran (control computation as well as plotting of the graphics) at a rate of about 1 Hz on a machine with 2.1 GHz processor and 3 Gb memory.

Figure 14 shows a similar example of coverage on a 2-torus with 2 obstacles by 5 robots. The matrix representation of the metric tensor on the torus is given by $\eta_{\bullet\bullet} = \begin{bmatrix} r^2 & 0 \\ 0 & (R + r\cos x)^2 \end{bmatrix}$, where R is the radius of the axial circle, r the radius of the *tube* of the torus, x is the *latitudinal* angle, and y is the *longitudinal* angle. Note how the Voronoi tessella (distinguished by the shades of green) in this case are not simply connected.

4.2 Application to Cooperative Exploration and Coverage Problem

Next we apply the tools developed to the problem of cooperative exploration and simultaneous coverage. In previous work [Bhattacharya 10] we had used an approximate and ad hoc "projection of centroid" method in order to compute an analog of *generalized centroid* and device a control law that was essentially to follow the approximate generalized centroid. However, now that we are equipped with the control law of Equation (8), we can achieve the same objectives in a more systematic way.

As detailed in [Bhattacharya 10], we choose the Shannon entropy for constructing the density

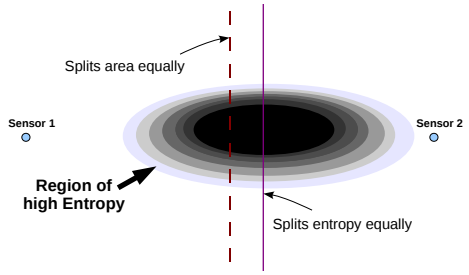

Figure 15: Entropy-weighted metric for voronoi tessellation in exploration problem.

function as well as to weigh the metric (Figure 15). Thus, if $p(\mathrm{q})$ is the probability that the vertex q is inaccessible (*i.e.* occupied or part of an obstacle), for all $\mathrm{q} \in \mathcal{V}(G)$, then the Shannon entropy is given by $e(\mathrm{q}) = -\left(p(\mathrm{q})\ln(p(\mathrm{q})) + (1-p(\mathrm{q}))\ln(1-p(\mathrm{q}))\right)$. We use this for modeling the discretized version of the weight function, $\overline{w}$, and an isotropic metric, ζI (where I is the identity matrix). Noting that in an exploration problem, the occupancy probability, p, and hence the entropy e, will be functions of time as well, we use the following formulae for $\overline{w}$ and ζ,

$$\overline{w}(\mathrm{q},t) = \begin{cases} \epsilon_{\overline{w}}, \text{ if } e(\mathrm{q},t) < \tau \\ e(\mathrm{q},t), \text{ otherwise.} \end{cases}, \qquad \zeta(\mathrm{q},t) = \begin{cases} \epsilon_{\zeta}, \text{ if } e(\mathrm{q},t) < \tau \\ e(\mathrm{q},t), \text{ otherwise.} \end{cases} \tag{9}$$

for some small $\epsilon_{\overline{w}}$ and ϵ_{ζ} representing zero (for numerical stability).

Each mobile robot maintains, updates and communicates a probability map for the discretized environment and updates its entropy map. We use a sensor model similar to that described in [Bhattacharya 10], and 'freeze' a vertex to prevent any change to its probability value when its entropy drops below some τ' $(< \tau)$.

In addition, to avoid situations where a robot gets stuck at a local minima inside its tessella even when there are vertices with entropy greater than τ in the tessella (this can happen when there are multiple high entropy regions in the tessella that exert equal and opposite pull on the robot so that the net velocity becomes zero), we perform a check on the value of the integral of the weight function, $\overline{w}$, within the tessella of the k^{th} robot when its control velocity vanishes. If the integral is above the value of $\int_{V_k} \epsilon_{\overline{w}}\, \mathrm{dq}$, we switch to a greedy exploration mode where the k^{th} robot essential head directly towards the closest point that has entropy greater than the value of τ. This ensures exploration of the entire environment (*i.e.* the entropy value for every accessible vertex drops below τ). And once that is achieved, both $\overline{w}$ and ζ become independent of time. Thus convergence is guaranteed.

Figure 16 shows screenshots of a team of 4 robots exploring a part of the 4^{th} floor of the Levine building at the University of Pennsylvania. The intensity of white represents the value of entropy. Thus in Figure 16(a) the robots start with absolutely no knowledge of the environment (maximum entropy), explore the environment, and finally converge to a configuration attaining coverage and minimum entropy (Figure 16(d)).

Figure 17 shows a similar scenario. However, in this case a human operator chooses to take control of one of the robots (Robot 0, marked by red circle) soon after they start cooperative exploration of the environment. That robot is forced to stay inside the larger room at the bottom of the environment. Moreover, in this case we use a team of heterogeneous robots (robots with different sensor footprint radii), thus requiring a *power voronoi tessellation*. This simple example illustrates the flexibility of our framework with respect to incorporating human inputs to guide exploration.

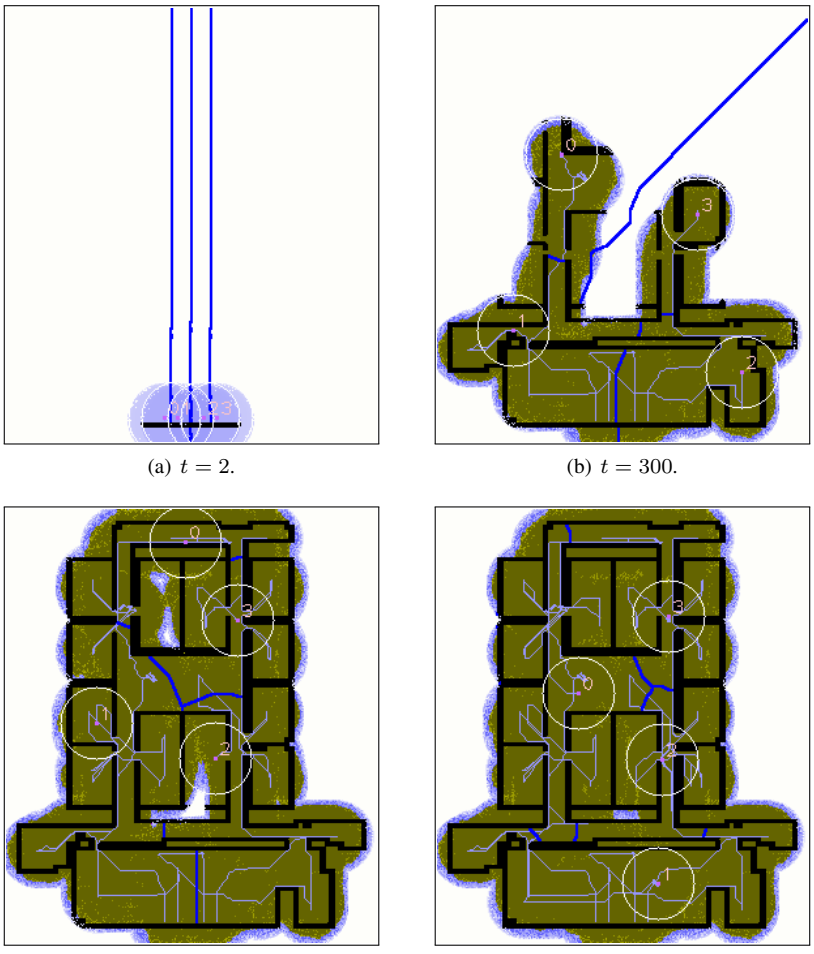

(a) $t = 2$.

(b) $t = 300$.

(c) $t = 900$.

(d) $t = 1550$. Converged solution.

Figure 16: Exploration and coverage of an office environment by a team of 4 robots. Blue curves indicate boundaries of tessellation, intensity of white indicates the value of entropy. Also see Extension 1.

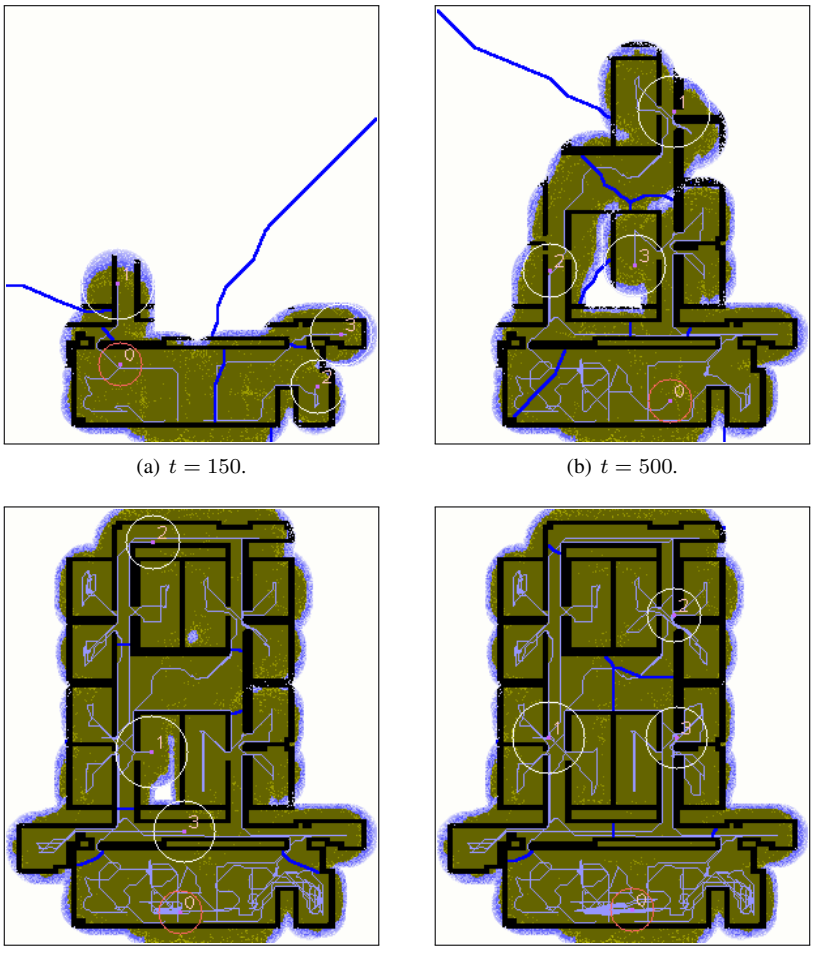

(a) $t = 150$. (b) $t = 500$.

(c) $t = 1450$. (d) $t = 2100$. Converged solution.

Figure 17: Exploration and coverage of an office environment discretized into a 284×333 grid by a team of 4 robots, with one of the robots (marked by red circle) being controlled by a human user. Also see Extension 1.

For either of the above examples, with the environment was discretized into a 284×333 grid, the program ran at a rate of about $3 - 4$ Hz on a machine with 2.1 GHz processor and 3 Gb memory.

5 Conclusion

In this paper we have extended the coverage control algorithm proposed by *Cortes, et al.* [Cortes 04], to non-Euclidean configuration spaces that are, in general, non-convex. The key idea is the transformation of the problem of computing gradients of distance functions to one of computing tangents to geodesics. We have shown that this simplification allows us to implement our coverage control algorithm in any space after reducing it to a discrete graph. We have illustrated the algorithm by considering multiple robots achieving uniform coverage on a 2-sphere and an indoor environment with walls and obstacles. We have also shown the application of the basic ideas to the problem of multi-robot cooperative exploration of unknown or partially known environments.

Acknowledgements

We gratefully acknowledge the support of the Office of Naval Research [grant numbers N00014-07-1-0829 and N00014-09-1-1031], the Army Research Laboratory [grant number W911NF-10-2-0016] and the Air Force Office of Scientific Research [grant number FA9550-10-1-0567].

Appendix: Proofs

Sketch of proof for Lemma L1:

> Since Ω is a manifold with C^1 boundaries, the 'neighborhood' of every $p \in \Omega$ will either resemble a complete Euclidean space (Figure 4(a)) or an Euclidean half space (Figure 4(b)). More technically, a λ-scaling of Ω at p will converge to $\mathbb{R}^N$ or $\mathbb{H}^N$ as $\lambda \to \infty$, where N is the topological dimension of Ω (see Proposition 3.15 of [Gromov 99]). This indeed is a convex cone in $T_{i(p)}\mathbb{R}^D$ (which, by definition, is λ-scaling of $\mathbb{R}^D$ at $i(p)$). To prove that this space is $T_p\Omega$, we just invoke the local connectedness property of $\mathbb{R}^N$ or $\mathbb{H}^N$, and hence existence of paths emanating from p that 'fill' the space. ■

Proof of Lemma L2:

> An Ω that can be represented as a subset of a smooth, complete manifold of same dimension, along with the described path metric d_ℓ, is sometimes referred to as a *metric space of type* (Δ) (see Theorem 2.1 of [Wolter 85]).
>
> i. The first result follows from the construction of the cut locus (see discussion in p. 42 of [Wolter 85]).
>
> ii. The fact that g_p is C^1 in $\Omega - (\partial\Omega \cup p \cup \mathcal{C}_p)$ follows from Theorem 3.1.b of [Wolter 85] (see Figure 5(a)). In fact a stronger condition holds: The gradient of g_p is locally Lipschitz continuous in $\Omega - (\partial\Omega \cup p \cup \mathcal{C}_p)$ (by Theorem 5.1 of [Wolter 85]).
>
> iii. If we choose $q, q' \in \Omega - (\partial\Omega \cup p \cup \mathcal{C}_p)$ at a distance of ϵ from each other, then due to the triangle inequality for the metric d_ℓ, we have $|g_p(q) - g_p(q')| \leq \epsilon$. Thus it follows that the gradient of g_p is bounded.
>
> ■

Sketch of proof for Lemma L3:

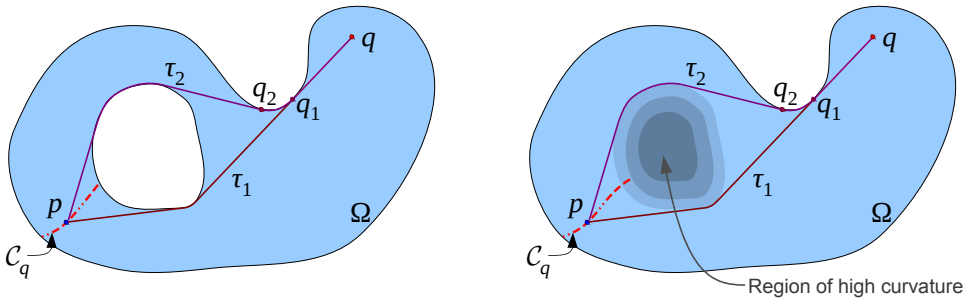

(a) Illustration for Lemma L3, adapted from Figure 3.1 of [Wolter 85].

(b) The same phenomenon can be created due to locally non-Euclidean metric on manifold with boundary.

Figure 18: Examples where $q \notin \mathcal{C}_p$, but $p \in \mathcal{C}_q$. This is because the minimal paths, τ_1 and τ_2, have parallel tangents at q.

First we note that, unlike the case in complete manifolds (Lemma 2 of [Klingenberg 59]), the statement is not true in general for every p on a manifold with boundaries. For an example refer to Figure 3.1 of [Wolter 85] or Figure 18. Thus, the main objective is to prove that the set of points for which the statement is not true is a set of measure zero in Ω. For the purpose of this sketch we assume that the boundary of Ω is smooth. However, this can be relaxed without too much difficulty.

We consider the set of points, $\mathcal{D}_\Omega \subset \Omega$, for which the statement within quotes is not true. Let $p \in \mathcal{D}_\Omega$ and $q \notin \mathcal{C}_p$ but $p \in \mathcal{C}_q$. Thus the two minimal paths (say τ_1 and τ_2) connecting p and q should have parallel tangents at q but distinct tangents at p. For that being possible, one of the minimal paths (say τ_1) needs to be tangent at some point $q_1 \in \partial\Omega$ to $\partial\Omega$, where the two distinct tangents emanating from p meet parallely for the first time (and hence continue together up to q). For the two paths to be distinct before q_1, the other minimal path (τ_2) needs to meet the boundary earlier than q_1, and 'graze' the boundary up to q_1 – say it meets at $q_2 \in \partial\Omega$ (see Figure 18). Clearly, the part of τ_2 connecting q_1 and q_2 has to be a geodesic segment on $\partial\Omega$.

Let Ω be of dimension N. A choice of the point p and two directions for the paths emanating from p is equivalent to choosing a point on the double sphere bundle $\mathcal{S}\Omega := \Omega \times \mathbb{S}^{N-1} \times \mathbb{S}^{N-1}$. Let the point p, along with the tangents to τ_1 and τ_2 at p (which we represent as t_1 and t_2 respectively), be represented on $\mathcal{S}\Omega$ by the triple (p, t_1, t_2). Now, we look at the tangent space of $\mathcal{S}\Omega$ at (p, t_1, t_2) and determine the dimension of the subspace along which we can perturb the position of the point p and the directions of the emanating minimal paths (*i.e.* t_1 and t_2) such that the aforesaid conditions are satisfied. We write $T_{(p,t_1,t_2)}\mathcal{S}\Omega$ for that tangent space, which is of dimension $N + 2(N-1) = 3N - 2$, with $T_p\Omega$ regarded as a N-dimensional subspace.

We consider the case where τ_j $(j = 1, 2)$ do not touch $\partial\Omega$ between p and q_j (like the scenario in Figure 18(b), but unlike the scenario in Figure 18(a)). It can be easily verified that the situations in which they do, result in additional constraints that further reduces the number of orthogonal directions in which (p, t_1, t_2) can be perturbed. The case that we consider here can arise, for example, when the central hole/obstacle in Figure 18(a) is removed, but is replaced by a region of high curvature as in Figure 18(b).

First, in order to maintain tangency of τ_1 at q_1 with $\partial\Omega$, the perturbations will need to satisfy 1 constraint. That gives us a $(3N-2)-1 = 3N-3$ dimensional subspace of $T_{(p,t_1,t_2)}\mathcal{S}\Omega$ in which we can test our further perturbations. Now consider the geodesic curve on $\partial\Omega$ emanating from q_1 and along the direction of the tangent of τ_1 at q_1. For τ_2 to intersect this curve, we have another $N-2$ constraints (there would be 0 constraints to intersect any arbitrary point on the $N-1$ dimensional $\partial\Omega$. Thus to intersect a 1 dimensional submanifold of it, we need to impose $(N-1)-1$ constraints). This point of intersection is q_2. Further, in order to ensure that the tangent to τ_2 at q_2 is parallel to the geodesic segment connecting q_1 and q_2 at q_2, we will need to impose another $N-1$ constraints (since the space of possible directions in which

it is possible to pass through q_2 is $\mathbb{S}^{N-1}$, and we need τ_2 to be tangent to a specific direction at q_2). Thus, so far, we have $1+(N-2)+(N-1) = 2N-2$ constraints, that leaves us with a $(3N-2)-(2N-2) = N$ dimensional subspace of $T_{(p,t_1,t_2)}\mathcal{S}\Omega$ along which we can choose a direction to move (p, t_1, t_2) ans still satisfy the required conditions. Finally, we need to impose the constraint that the lengths of the paths τ_1 and τ_2 need to be equal. This imposes 1 additional constraint. Thus, the dimensionality of the subspace of $T_{(p,t_1,t_2)}\mathcal{S}\Omega$ along which we can perturb the point p and the emanating directions of τ_1 and τ_2 is $N-1$. Even if this subspace lies entirely in $T_p\Omega \subset T_{(p,t_1,t_2)}\mathcal{S}\Omega$, it is one dimension less than the dimensionality of $T_p\Omega$. Thus the dimensionality of $\mathcal{D}_\Omega$ can at most be $N-1$. ■

As discussed earlier, we first prove Lemma L4 and Corollary C1, using which we will prove the Proposition P1.

It is possible to prove Lemma L4 using more direct arguments that establish the direction of steepest descent of a function in the tangent space as the dual of the differential of the function (*i.e.* gradient of a function). However, for completeness, we provide an explicit proof.

Proof of Lemma L4:

For notational convenience, let us define $g_{\mathbf{w}}(\mathbf{u}) := d^C(\mathbf{w}, \mathbf{u}),\ \forall \mathbf{u} \in Img(\phi)$. Recall that geodesically convex implies that any two points in U can be connected using a smooth geodesic segment (a curve satisfying the geodesic equation at every point) lying entirely in U.

Consider $g_{\mathbf{w}}$ as a function from $\mathbb{R}^D$ to $\mathbb{R}_+$ with an unique minima at $\mathbf{w}$. Let $\gamma_{\mathbf{wq}}$ represents any arbitrary curve in $Img(\phi) \subseteq \mathbb{R}^D$ connecting $\mathbf{w}$ to $\mathbf{q}$. By the *fundamental theorem of calculus* and using the fact that $g_{\mathbf{w}}(\mathbf{w}) = 0$, we have,

$$I(\gamma_{\mathbf{wq}}) \ := \ g_{\mathbf{w}}(\mathbf{q}) \ = \ \int_{\gamma_{\mathbf{wq}}} \frac{\partial}{\partial \mathbf{u}} g_{\mathbf{w}}(\mathbf{u}) \cdot \mathrm{d}\mathbf{u} \ \equiv \ \int_{\gamma_{\mathbf{wq}}} \frac{\partial g_{\mathbf{w}}(\mathbf{u})}{\partial u^i} \, \mathrm{d}u^i \tag{10}$$

where, $[\,\mathrm{d}u^1, \mathrm{d}u^2, \cdots, \mathrm{d}u^D]$ is the coefficient vector (in chart C) of an infinitesimal element along the tangent to the curve.

Now, the length of the curve $\gamma_{\mathbf{wq}}$ is given by

$$L(\gamma_{\mathbf{wq}}) \ := \ \int_{\gamma_{\mathbf{wq}}} \sqrt{\eta_{ij}(\mathbf{u}) \ \mathrm{d}u^i \, \mathrm{d}u^j} \tag{11}$$

By definition, the value of $L(\gamma_{\mathbf{wq}})$ is minimum when $\gamma_{\mathbf{wq}}$ is the shortest geodesic (which, due to the hypothesis that the cut locus of any point in U is empty, is unique – call it $\gamma^*_{\mathbf{wq}}$) connecting $\mathbf{w}$ and $\mathbf{q}$, and the minimum value is clearly $g_{\mathbf{w}}(\mathbf{q})$ (by definition of $g_{\mathbf{w}}$). Thus,

$$\begin{gathered} L(\gamma_{\mathbf{wq}}) \ \geq \ I(\gamma_{\mathbf{wq}}) \ \ [= g_{\mathbf{w}}(\mathbf{q}), \text{ a const. independent of } \gamma_{\mathbf{wq}}] \ , \\ \text{equality holds when } \gamma_{\mathbf{wq}} = \gamma^*_{\mathbf{wq}} \end{gathered} \tag{12}$$

Now, consider a family of infinitesimal elements of $\mathbb{R}^D$ represented by the coefficient vector $\mathrm{d}\mathbf{u} = [\,\mathrm{d}u^1, \ \mathrm{d}u^2, \cdots, \ \mathrm{d}u^D]^T$ located at an arbitrary point $\mathbf{u} \in Img(\phi)$ such that $\mathbf{u} + \mathrm{d}\mathbf{u}$ lies inside $Img(\phi)$. From the triangle inequality of d^C (since it is induced by a Riemannian metric) we have,

$$\begin{aligned} & d^C(\mathbf{w}, \mathbf{u} + \mathrm{d}\mathbf{u}) \ \leq \ d^C(\mathbf{w}, \mathbf{u}) + d^C(\mathbf{u}, \mathbf{u} + \mathrm{d}\mathbf{u}) \\ \implies & d^C(\mathbf{w}, \mathbf{u} + \mathrm{d}\mathbf{u}) - d^C(\mathbf{w}, \mathbf{u}) \ \leq \ d^C(\mathbf{u}, \mathbf{u} + \mathrm{d}\mathbf{u}) \\ \implies & \frac{\partial}{\partial \mathbf{u}} g_{\mathbf{w}}(\mathbf{u}) \Big|_{\mathbf{u}} \cdot \mathrm{d}\mathbf{u} \ \leq \ \sqrt{\eta_{ij}(\mathbf{u}) \ \mathrm{d}u^i \, \mathrm{d}u^j} \\ \implies & \frac{\partial g_{\mathbf{w}}(\mathbf{u})}{\partial u_i} \, \mathrm{d}u^i \ \leq \ \sqrt{\eta_{ij}(\mathbf{u}) \ \mathrm{d}u^i \, \mathrm{d}u^j} \ = \frac{\eta_{ij}(\mathbf{u}) \, \mathrm{d}u^i \, \mathrm{d}u^j}{\sqrt{\eta_{mn}(\mathbf{u}) \ \mathrm{d}u^m \, \mathrm{d}u^n}} \end{aligned} \tag{13}$$

Equality of the triangle inequality in (13) of course holds when $\mathbf{u}$ lies on the geodesic connecting $\mathbf{w}$ and $\mathbf{u} + \mathrm{d}\mathbf{u}$.

Now consider a curve $\gamma'_{\mathbf{wq}}$ (connecting $\mathbf{w}$ and $\mathbf{q}$) with infinitesimal elements $\mathrm{d}\mathbf{u}$ along the tangents to the curve. If there exists at least one point along that curve on which the inequality in (13) is not an equality, then the integrals of the quantities on the two sides of the inequality will not be equal. That is, for such a curve we will have $I(\gamma'_{\mathbf{wq}}) < L(\gamma'_{\mathbf{wq}})$.

But we know that there does exist a curve, $\gamma^*_{\mathbf{wq}}$, such that $I(\gamma^*_{\mathbf{wq}}) = L(\gamma^*_{\mathbf{wq}})$ does hold. Thus, for that curve it should be true that at each and every point of the curve the equality of (13) holds true. Thus we have essentially shown that for the geodesic, $\gamma^*_{\mathbf{wq}}$, at each and every point of the curve the following holds

$$\frac{\partial g_{\mathbf{w}}(\mathbf{u})}{\partial u_i}\,\mathrm{d}u^i \;=\; \frac{\eta_{ij}(\mathbf{u})\,\mathrm{d}u^i\,\mathrm{d}u^j}{\sqrt{\eta_{mn}(\mathbf{u})\;\mathrm{d}u^m\,\mathrm{d}u^n}}$$

where $\mathrm{d}\mathbf{u}$ are of course infinitesimal elements at $\mathbf{u}$ along the tangent to $\gamma^*_{\mathbf{wq}}$.

One can normalize by dividing by $\|\,\mathrm{d}\mathbf{u}\|_2$ to obtain

$$\frac{\partial g_{\mathbf{w}}(\mathbf{u})}{\partial u_i} z^i_{\mathbf{qu}} \;=\; \frac{\eta_{ij}(\mathbf{u}) z^i_{\mathbf{qu}} z^j_{\mathbf{qu}}}{\sqrt{\eta_{mn}(\mathbf{u})\; z^m_{\mathbf{qu}} z^n_{\mathbf{qu}}}} \tag{14}$$

where $z^i_{\mathbf{qu}}$ is the i^{th} component of the tangent vector at $\mathbf{u}$ to the geodesic connecting $\mathbf{w}$ to $\mathbf{u}$, which due to our assumption is unique. We note that the right-hand-side of the above equation represents a scalar field (call it S). Also, $z^i_{\mathbf{qu}}$ (which are functions of $\mathbf{u}$) represent the coefficients of a contravariant vector field in $(U - \mathbf{w})$. Thus, writing X_i for $\frac{\partial g_{\mathbf{w}}(\mathbf{u})}{\partial u_i}$, one can rewrite Equation (14) as

$$X_i z^i_{\mathbf{qu}} = S(\mathbf{u}) \tag{15}$$

where we need to solve for the coefficients $X_i(\mathbf{u}) := \frac{\partial g(\mathbf{u})}{\partial u_i}$. Of course a particular solution is

$$X_{0,i}(\mathbf{u}) = \frac{\eta_{ij}(\mathbf{u}) z^j_{\mathbf{qu}}}{\sqrt{\eta_{mn}(\mathbf{u})\; z^m_{\mathbf{qu}} z^n_{\mathbf{qu}}}} \tag{16}$$

These coefficients clearly transform as coefficients of a covariant vector field. Moreover, the contravariant vector field corresponding to this covariant field (*i.e.* the vectors with coefficients $X^{0,i} = \eta^{ij} X_{0,j}$) is parallel to $z^i_{\mathbf{qu}}$. From this we can infer that the solution mentioned in (16) is the only solution of (15) that transforms as coefficients of a covariant vector field (This is because of the following: Every covariant transformation of X_i corresponds to an unique contravariant transformation of X^i. Again, the general solutions of X^i need to be such that $\eta_{ij} z^i_{\mathbf{qu}} X^j = \eta_{ij} z^i_{\mathbf{qu}} X^{0,j} = \beta \eta_{ij} z^i_{\mathbf{qu}} z^j_{\mathbf{qu}}$ for some scalar field β. This needs to be true in every coordinate chart. Due to positive definiteness of $\eta_{\bullet\bullet}$, this is possible only with X^j parallel to $z^j_{\mathbf{qu}}$, which also fixes the scalar multiple β since we have the known scalar field, S.).

Thus we have

$$\frac{\partial g_{\mathbf{w}}(\mathbf{u})}{\partial u_i} = \frac{\eta_{ij}(\mathbf{u}) z^j_{\mathbf{qu}}}{\sqrt{\eta_{mn}(\mathbf{u})\; z^m_{\mathbf{qu}} z^n_{\mathbf{qu}}}} \tag{17}$$

Thus, by specializing for $\mathbf{u} = \mathbf{q}$, we obtain the proposed result. ■

Proof of Corollary C1:

We first note that due to Lemma L2, we can always choose an open neighborhood of q, $\mathcal{B}_q \subseteq V$, which is geodesically convex, on which the function $g_p := d_\ell(p, \cdot)$ is of class C^1, and the cut locus of every point in which is empty in $\mathcal{B}_q$ (since $q \notin \mathcal{C}_q$).

Consider a minimal path γ^*_{pq} connecting p and q. Let $w(\neq q)$ be a point on this path (between p and q) that lies inside $\mathcal{B}_q$ (which we can always find since $\mathcal{B}_q$ is open) – see Figure 8(a).

From the definition of minimal path we have $\gamma^*_{pq} = \gamma^*_{pw} \cup \gamma^*_{wq}$, for a minimal path, γ^*_{pw}, connecting p and w, and the minimal geodesic, γ^*_{wq}, connecting w and q (which is unique since $q \notin \mathcal{C}_p$). Thus it follows that,

$$\mathbf{z}_{p\mathbf{q}} = \mathbf{z}_{w\mathbf{q}} \tag{18}$$

Again, by triangle inequality, for any $\mathbf{u} \in \psi(\mathcal{B}_q)$

$$\begin{aligned} & d^{\tilde{D}}_\ell(p, \mathbf{u}) \;\leq\; d_\ell(p, w) + d^{\tilde{D}}_\ell(w, \mathbf{u}) \\ \Rightarrow \quad & g_p(\mathbf{u}) \;\leq\; h(\mathbf{u}) \end{aligned} \tag{19}$$

where $h(\mathbf{u}) := d_\ell(p, w) + d^{\tilde{D}}_\ell(w, \mathbf{u})$ and $g_p(\mathbf{u}) := d^{\tilde{D}}_\ell(p, \mathbf{u})$.
However, equality does hold when p, w and $\psi^{-1}(\mathbf{u})$ lie on the same shortest path. This, in particular, is true when $\mathbf{u} = \mathbf{q}$ (due to our choice of w). Now, since $q \notin \mathcal{C}_p$ and by our choice of $\mathcal{B}_q$, both g_p and h are of class C^1 at $\mathbf{q}$. Thus we have $g_p(\mathbf{u}) \leq h(\mathbf{u})$ for $\mathbf{u} \in \psi(\mathcal{B}_\mathbf{q})$, and at $\mathbf{u} = \mathbf{q}$ they satisfy equality and are differentiable. This implies the differentials of the functions at $\mathbf{q}$ should be same,

$$\begin{aligned} & \frac{\partial}{\partial \mathbf{u}} g_p(\mathbf{u})\Big|_{\mathbf{u}=\mathbf{q}} \;=\; \frac{\partial}{\partial \mathbf{u}} h(\mathbf{u})\Big|_{\mathbf{u}=\mathbf{q}} \\ \Rightarrow \quad & \frac{\partial}{\partial \mathbf{u}} d^{\tilde{D}}_\ell(p, \mathbf{u})\Big|_{\mathbf{u}=\mathbf{q}} \;=\; \frac{\partial}{\partial \mathbf{u}} d^{\tilde{D}}_\ell(w, \mathbf{u})\Big|_{\mathbf{u}=\mathbf{q}} \end{aligned} \tag{20}$$

Now, $\mathcal{B}_q$ satisfies the conditions for U in Lemma L4, and w and q are points inside it. Thus by Lemma L4,

$$\frac{\partial}{\partial u^i} d^{\tilde{D}}_\ell(w, \mathbf{u})\Big|_{\mathbf{u}=\mathbf{q}} \;\equiv\; \frac{\partial}{\partial u^i} d^{D}_\ell(\mathbf{w}, \mathbf{u})\Big|_{\mathbf{u}=\mathbf{q}} \;=\; \frac{\eta_{ij}(\mathbf{q})\; z^j_{w\mathbf{q}}}{\sqrt{\eta_{mn}(\mathbf{q})\; z^m_{w\mathbf{q}} z^n_{w\mathbf{q}}}} \tag{21}$$

where $\mathbf{w} = \psi(w)$.

Substituting from (18) and (20) into (21) we obtain the proposed result. ■

Proof of Proposition P1:

Equipped with Corollary C1 we can now conclude the proof of Proposition P1. The gradient of a function is, by definition, the dual of the differential, *i.e.* $\text{grad}(f) = \left(\frac{\partial f}{\partial x^i}\, \mathrm{d}x^i\right)^* = \eta^{ij} \frac{\partial f}{\partial x^j} \frac{\partial}{\partial x^i}$. Let q be a point on $\partial\Omega$ and $\{q_i\}$ be a Cauchy sequence of points converging to q. Due to Corollary C1, at every point $q_i \in \Omega - (\partial\Omega \cup p \cup \mathcal{C}_p)$, the negative of the gradient of the distance from p is parallel to $-z_{pq_i}$, the tangent at q_i to the minimal path connecting q_i to p (Figure 6). Due to our definition of gradient at boundary points, the gradient of the distance function at q will then be $\lim_{i\to\infty} -z_{pq_i}$. Since d_ℓ is a path metric, the minimal path connecting each q_i to p exists in Ω, as does the path connecting q to p. Thus, the limit exists in $T_q\Omega$. ■

References

[Alexander 81] S. Alexander. *Distance geometry in Riemannian manifolds-with-boundary*. vol. 838, pages 12–18, 1981.

[Bhattacharya 10] S. Bhattacharya, N. Michael & V. Kumar. *Distributed coverage and exploration in unknown nonconvex environments*. In Proceedings of the 10th International Symposium on Distributed Autonomous Robotics Systems, pages 1–14. Springer, 2010.

[Bullo 09] F. Bullo, J. Cortés & S. Martínez. Distributed control of robotic networks: A mathematical approach to motion coordination algorithms. Applied Mathematics Series. Princeton University Press, 2009.

[Cormen 01] Thomas H. Cormen, Clifford Stein, Ronald L. Rivest & Charles E. Leiserson. Introduction to algorithms. McGraw-Hill Higher Education, 2001.

[Cortes 04] J. Cortes, S. Martinez, T. Karatas & F. Bullo. *Coverage control for mobile sensing networks*. IEEE Trans. Robot. Autom., vol. 20, no. 2, pages 243–255, April 2004.

[Cortez 04] Jorge Cortez, Sonia Martinez, Timur Karatas & Francesco Bullo. *Coverage Control for Mobile Sensing Networks*. IEEE Trans. Robot. and Automat., vol. 20, no. 2, pages 243–255, 2004.

[Cortez 05] Jorge Cortez, S. Martinez & Francesco Bullo. *Spatially-distributed coverage optimization and control with limited-range interactions*. ESIAM: Control, Optimisation and Calculus of Variations, vol. 11, pages 691–719, 2005.

[Cundy 89] H. Cundy & A. Rollett. Mathematical models. Tarquin Pub., 3rd edition, 1989.

[Dijkstra 59] Edsger W. Dijkstra. *A note on two problems in connexion with graphs*. Numerische Mathematik, vol. 1, pages 269–271, 1959.

[Durham 12] J.W. Durham, R. Carli, P. Frasca & F. Bullo. *Discrete Partitioning and Coverage Control for Gossiping Robots*. IEEE Transactions on Robotics, vol. 28, no. 2, pages 364–378, 2012.

[Gromov 99] M. Gromov, J. Lafontaine & P. Pansu. Metric structures for riemannian and non-riemannian spaces. Progress in mathematics. Birkhäuser, 1999.

[Jost 97] J. Jost. Compact riemann surfaces. Springer-Verlag, 1997.

[Klingenberg 59] W. Klingenberg. *Contributions to Riemannian Geometry in the Large*. Annals of Mathematics, vol. 69, no. 3, pages 654–666, May 1959.

[Lloyd 82] Stuart P. Lloyd. *Least squares quantization in PCM*. IEEE Trans. Inf. Theory, vol. 28, pages 129–137, 1982.

[Lozano-Pérez 79] Tomás Lozano-Pérez & Michael A. Wesley. *An algorithm for planning collision-free paths among polyhedral obstacles*. Commun. ACM, vol. 22, no. 10, pages 560–570, October 1979.

[Munkres 99] James Munkres. Topology. Prentice Hall, 1999.

[Petersen 06] P. Petersen. Riemannian geometry. Graduate Texts in Mathematics. Springer, 2006.

[Pimenta 08] L. C. A. Pimenta, V. Kumar, R. C. Mesquita & G. A. S. Pereira. *Sensing and Coverage for a Network of Heterogeneous Robots*. In Proc. of the IEEE Conf. on Decision and Control, pages 3947–3952, Cancun, Mexico, December 2008.

[Rimon 92] E. Rimon & D.E. Koditschek. *Exact Robot Navigation Using Artificial Potential Fields*. IEEE Transactions on Robotics and Automation, vol. 8, no. 5, pages 501–518, 1992.

[Sastry 99] S. Sastry. Nonlinear systems: Analysis, stability and control. Interdisciplinary applied mathematics: Systems and control. Springer, 1999.

[Stachniss 05] C. Stachniss, G. Grisetti & W. Burgard. *Information Gain-based Exploration Using Rao-Blackwellized Particle Filters*. In Proc. of Robot.: Sci. and Syst., pages 65–72, Cambridge, MA, June 2005.

[Stachniss 06] C. Stachniss. *Exploration and Mapping with Mobile Robots*. PhD thesis, University of Freiburg, Freiburg, Germany, April 2006.

[Thrun 05] Sebastian Thrun, Wolfram Burgard & Dieter Fox. Probabilistic robotics (intelligent robotics and autonomous agents). The MIT Press, 2005.

[Wolter 85] Franz-Erich Wolter. *Cut loci in bordered and unbordered Riemannian manfolds*. PhD thesis, Department of Mathematics, Technical University of Berlin, 1985.